https://ntrs.nasa.gov/search.jsp?R=19790005232 2020-03-22T00:57:07+00:00Z

NASA Technical Memorandum 78628

(NASA-TM-78628) BUCKLING TESTS OF STRUCTURAL ELEMENTS APPLICABLE TO LARGE ERECTABLE SPACE TRUSSES (NASA) 61 p HC A04/MF A01 CSCL 20K

N79-13403

G3/39 Unclas 39031

BUCKLING TESTS OF STRUCTURAL ELEMENTS APPLICABLE TO LARGE ERECTABLE SPACE TRUSSES

W. L. Heard, Jr., H. G. Bush, and Nancy Agranoff

October 1978

NASA
National Aeronautics and Space Administration

Langley Research Center
Hampton, Virginia 23665

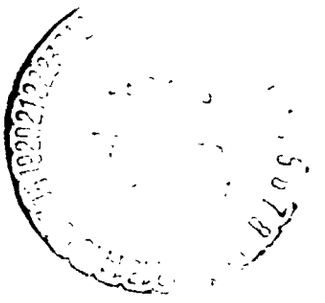

INTRODUCTION

Truss type structures are receiving considerable attention for application as large-area, low-mass, space platforms. These platforms would serve to support the functional equipment required for future space missions being considered by NASA such as solar energy collection, communications antennas, and earth resources surveillance. The octetruss (tetrahedral truss) structure (refs. 1 & 2) is one promising concept for this application, and the nestable, tapered, graphite-epoxy (Gr/E) column described in reference 3 is an attractive candidate for use as the prime element of an erectable type octetruss. Due to their nesting characteristics, these columns may be packaged tightly for efficient transportation into orbit via Space Shuttle flights (ref. 3). They are also highly efficient compression members and can be designed to have small thermal expansion characteristics.

The nestable column concept for truss structure elements, however, not only requires the usual engineering concern for some type of stable "cluster joint" at nodes where multiple truss elements converge at a point, but has the additional requirement for a "center joint" in the middle of each of the truss elements. Since Gr/E elements of large space truss platforms will function as long slender columns in an extremely low strain range (ref. 4), it is important to investigate the effect of such joints on stability behavior as well as assess the validity of using, for analysis predictions, standard material properties for Gr/E determined from coupons tested under much larger strain ranges.

Some preliminary buckling test results for two Gr/E nestable columns have already been presented in reference 4. The purpose of the present paper is to present detailed data on the columns and center joint of reference 4 for completeness, and to present buckling data for additional columns as well as a tripod arrangement of these columns using a cluster joint. The objectives of these tests are: (1) to gain insight into joint requirements for truss structures, (2) to assess the structural qualities of the column and center joint designs, (3) to investigate the restraint provided by octetruss core members (tripod) to the cluster joints, (4) to provide insight into the level of analysis required to predict buckling behavior of Gr/E nestable columns both as simple columns and in a tripod arrangement, and (5) to provide a data base for Gr/E nestable columns.

SYMBOLS

A	arbitrary constant (see eq. A(5))
$\tilde{A}$	cross-sectional area
a	length of truncated segment of tapered bar (see fig. 23)
B	arbitrary constant (see eq. A(5))
$b = a + \frac{\ell}{2}$	
$C = 4\frac{\rho a^3}{EI_{min}}$	
E	modulus of elasticity
E_{AL}	modulus of elasticity for aluminum
$E_{Gr/E}$	modulus of elasticity for graphite-epoxy
F	applied force at apex of tripod (see Table 7)
F_{cr}	buckling value of applied load at apex of tripod
I_{max}	maximum cross-sectional moment of inertia of uniform thickness tapered tube
I_{min}	minimum cross-sectional moment of inertia of uniform thickness tapered tube
I_x	moment of inertia of tube cross-section
J_0, J_1, J_{-1}	Bessel functions of the first kind
L	simply supported column length
$\bar{L}$	column specimen length

ℓ	half-column length
ℓ_i	segment lengths of half-columns (i = 1, 2, 3, 4, 5; see fig. 19)
$\bar{\ell}_i$	lengths of nestable half-columns joined to form complete column (i = 1, 2; see Table 1)
m	buckling factor for tapered tube column (see fig. 17)
P	axial load on column
P_{crit}	Euler buckling load of tapered tube column
r_{max}, r_{min}	maximum and minimum radii, respectively, of tapered tube (see fig. 23)
r_1, r_2	end radii of graphite-epoxy segment of half-column (see fig. 19)
$\bar{r}_0$, $\bar{r}_3$, $\bar{r}_4$, $\bar{r}_5$	average radii of segments of half-columns (see fig. 19)
t_i	wall thicknesses of segments of half-columns (i = 1, 2, 3, 4, 5; See fig. 19)
x,y	coordinates of tapered tube (see fig. 23)
Y_0, Y_1, Y_{-1}	Bessel functions of the second kind

$$\alpha = \frac{r_{min}}{r_{max}}$$

δ	average end-shortening of column
δ_{exp}	average measured end-shortening of column
ε	average axial strain
σ	average axial stress
ϕ	angle of applied load at apex of tripod (see Table 7)

DESCRIPTION OF TEST SPECIMENS

Composite Columns

The test specimens are doubly-tapered, tubular columns of graphite-epoxy (Gr/E) construction. The full column is assembled from two tapered, half-column elements (see sketch in Table 1) which are joined together at their large radii ends. Two different wall layups were used. The specimen designations, ply layups, dimensions and masses (including end fittings) are given in Table 1. Specimens designated C3, C4A, C4B, and C4C were tested as columns only, while those designated TA, TB, and TC were tested as columns as well as in a tripod arrangement. All of the specimens were fabricated on the same mandrel and thus have similar inside dimensions. Gores for the 0^{o} layers were cut (as shown in the sketch below Table 1) from 7.62 cm wide T300/5208 Gr/E, unidirectional, prepreg, tape which had a nominal cured thickness of 0.14 mm. The inner and outer 90^{o} layers were wound using 1.27 cm wide tape of the same material but having a nominal cured thickness of 0.076 mm. Nominal material properties are given in Table 2.

Center Joints

In the nestable column concept, the truss elements are manufactured in half-column lengths which can be nested into compact bundles containing many half-columns for Shuttle transportation as indicated in figure 1. The half-columns are assembled into full column elements after orbit is achieved. Thus, a center joint is required which is reliable and easy to

assemble. One plausible concept, originally presented in ref. 3 can be seen attached to the column in figure 1. This joint uses external interlocking leaf springs which are tapered to enhance alignment of the joint halves and requires only a simple translational motion for assembly. The detail configuration and operation of this joint may be seen more clearly in the three photographs in figure 2. Figure 2(a) shows the joint unassembled. In figure 2(b) assembly has been initiated, but the two identical halves must be pushed together before locking occurs. Figure 2(c) shows the joint fully assembled. As can be seen, use of external leaf springs permits visual inspection of the joint to verify that locking has occurred. All of the test specimens were fabricated with these identical center joints. The joints were fabricated from 7075 aluminum and bonded to the inside surface of the column during fabrication of the column.

End Joints

In addition to the center joint, the truss elements must also be provided with end joints capable of being joined in a nine element cluster typical of the octetruss. The concept used for the present tests is shown in two views in figure 3. The cylindrical clevis receiver sleeve to the extreme left in the two photographs is bonded to the inside surface of the Gr/E column during fabrication of the column. Next, a snap-in clevis joint using a steel snap-ring is used to form the transition from the column to the cluster joint shown at the extreme right in figure 3. (The cluster joint, of course was used only in the

tripod tests). The clevis joint is shown being inserted into the column (without the snap-ring) in figure 4(a). Figure 4(b) shows the clevis fully installed. This joint could easily have been made in one piece, but for laboratory test purposes a two piece joint was more advantageous since it allows different end-joint concepts to be used with the same column. All of the specimens tested were equipped with clevis type end fittings, except for specimens C3 and C4A which were fabricated prior to the design of the clevis joint and were equipped with a threaded stud as shown in figure 5.

Cluster Joint

A cluster joint is required where multiple column elements of a truss structure converge at a point. For the octetruss platform, a cluster joint must accomodate nine such elements. The cluster joint used in this investigation is shown in figure 3. It was designed to be lightweight and have small out-of-plane bending stiffness in each of the nine attachment legs to reduce thermal distortion of the truss. The joint is also required to permit installation of a "rigid" column element between two cluster joints fixed in space. Figure 6 indicates how the assembly is achieved. A column element with clevis joints attached to each end and properly oriented is brought into position so that the clevises lie between two adjacent legs of each of the two fixed cluster joints. (Only one of these joints is shown in figure 6). The entire column is then slipped to the side so that the clevis slides

over the cluster joint leg. The holes are then lined up and assembly is completed by inserting fasteners into the holes. It is anticipated that the use of fasteners would be restricted to laboratory tests only. Figure 7 shows a cluster joint installed for the tripod tests using bolts for the final assembly. Note that the restraint to the cluster joint provided by the six surface member columns, which would be present in an octetruss arrangement, was not simulated for this test. (The white frame in the photograph is the loading fixture). A summary of masses of all joint components is given in Table 3.

Column Initial Imperfections

Extensive measurements were taken to determine the initial imperfection shapes of columns C3 and C4A. The results are given in figure 8(a for column C3 and figure 8(b) for column C4A. As can be seen, column C3 had a mid-length initial imperfection of about 0.46 cm, whereas column C4A had essentially zero initial center deflection. It is shown in figure 8, that the mid-length initial imperfection is highly dependent upon the orientation of the half-columns at the time they are joined together. No detailed initial imperfection measurements were taken on any of the other columns, although maximum mid-length initial imperfection for columns TA, TB, and TC were measured and found to be .20 cm, .36 cm, and .22 cm, respectively.

TEST APPARATUS, INSTRUMENTATION, AND PROCEDURE

Simply Supported Column Buckling Tests

Column tests were performed on all test specimens with the columns mounted vertically in the loading fixture as shown in figure 9. Simple support of the columns was achieved by the use of ball-and-cup joints, shown in the photographs in fig. 10. For columns C4B, C4C, TA, TB, and TC special steel ball-type fittings were attached to the column clevis joints as shown in figure 10. The steel cup fittings were mounted to a load cell at the top end of the column and a hydraulic jack at the bottom end. Teflon film and lubrication were inserted between the ball and the cup to eliminate galling of the ball in the cup during the load cycle. For columns C3 and C4A, a steel cone with a ball end as shown in figure 11 was used.

The columns were loaded and end shortening was measured between two .476 cm thick aluminum plates located perpendicular to the centerline of the column at both ends (see figure 12 and figure 9). Measurements were taken by three Direct Current Displacement Transducers (DCDT's) located at each end, 120 degrees apart and 3.18 cm from the outside surface of the column wall on the end plates. All columns were loaded to buckling at least three times each to assess repeatability of the data.

Elastically Supported Column Buckling Tests

The cluster joints described previously (see figures 3, 6, and 7) will not provide true simple support end conditions to the tripod elements,

nor will the wall mounting brackets (Fig. 13) used for the tripod tests. Hence, in addition to the simply supported column tests, the elastic restraint of the aluminum "legs" of the cluster joint and the wall brackets was also investigated by column tests of tripod elements TA and TB. The support hardware and terminology used are shown in figure 13. The bracket support is identical to the wall mounting bracket used in the tripod tests. The blade support is representative of a leg of the cluster joint. Columns TA and TB were tested to buckling failure using various combinations of these end supports.

Tripod Buckling Tests

The tripod is shown mounted to the vertical wall test fixture in figure 7. The aluminum blade-type fitting used to support the tripod at the wall is shown in figure 13(b). The clevis joints of the tripod column elements were slipped over the blades of the fittings and bolts were inserted to secure the connections. The tripod was formed with columns TA, TB, and TC in the arrangement shown in figure 14. Each of the column elements were instrumented with three strain gages located 120^{o} apart at a longitudinal station near the midlength of the column.

The load was applied at the apex of the tripod and directed in a plane parallel to the base of the tripod. The load was produced by a hydraulic jack operating on a cable and pully system as shown schematically in figure 14. The direction of loading was varied by 30 increments by relocating the pulley as indicated.

The cluster joint described previously and shown in figures 3, 6, and 7 was designed for a 4450 N load which is representative of loads that may

occur in the surface elements of very large octetruss space structure (several square kilometers). Core members, of which the tripod is somewhat representative, would actually see only a fraction of this load. The tripod elements used in the tests, however, were originally sized to preclude buckling at loads up to 4450 N; hence, a stronger cluster joint had to be designed in order to buckle the tripod for all orientations of the load. A photograph of this joint is shown compared with the original cluster joint in figure 15. Note that the three legs which would be attached to the tripod columns are of the same thickness as the original cluster joint but that final machining to remove the material between the legs was not performed.

RESULTS AND DISCUSSION

Simply Supported Column Buckling Tests and Analysis

A representative load--end-shortening curve is shown in figure 16 for each specimen tested. In this type of figure, the curve for a slender column will asymptotically approach the column (Euler) buckling load as the end-shortening increases under loading. In figure 16, buckling loads calculated from the column buckling theory of reference 5 are compared with the test data. From this theory the buckling load for a doubly-tapered, laminated tube may be calculated from the following expression:

$$P_{crit} = \frac{mEI_{max}}{L^2} \qquad (1)$$

where E is Young's modulus of the laminate, I_{max} is the maximum moment of inertia of the tube, and L is the length. The quantity m is determined by the method of reference 5 and is given in figure 17 as a function of the ratio r_{min}/r_{max}. The development of the appropriate equations for the determination of m is given in Appendix A.

The buckling load can be expressed in terms of Et (a measure of the column axial stiffness) by substituting $\pi r_{max}^3 t$ for I_{max} in equation (1). The result is:

$$P_{crit} = \frac{m\pi E t r_{max}^3}{L^2} \qquad (2)$$

The calculations for the buckling loads in figure 16 are based on an Et of the column determined from the linear range of the load-end-shortening test data shown in the figure. The expression which relates Et of the doubly-tapered column to the measured load P and end-shortening δ is derived in Appendix B and given by equation B(8). As can be seen in figure 16, all columns show buckling loads in good agreement with the test results. An average theoretical buckling load is given for columns C4B, C4C, TA, TB, and TC (horizontal dashed line) since all of these columns exhibited similar load--end-shortening behavior. The individual calculated buckling loads are presented in Table 4. The data shown in figure 16 are taken from a given test of each specimen, however, data taken from successive buckling failure tests of each column exhibited excellent "repeatability." The fact that column C3 had a larger initial

imperfection than all the other columns is indicated by the earlier nonlinear behavior of the data for this specimen as compared to the more linear character of the data for all other columns up to loads near the buckling load. An unexpected result, evident in figure 16 is that all the columns with $[90/0_4/90]$ ply layups do not exhibit similar stiffnesses. The stiffness of column C4A tends to agree with the theoretical value based on nominal material and geometric properties while all of the remaining $[90/0_4/90]$ columns exhibit higher stiffness characteristics as indicated by the higher asymptotic and slope values compared to column C4A. In order to understand this behavior, several sample sections were cut from one of the stiffer specimens and examined under a microscope. It was found that many of the 0^o gores were overlapped longitudinally during fabrication of the specimens as indicated by the photograph in figure 18(a). The photograph is a microscopic view of a section with the 0^o graphite fibers oriented normal to the section. Five 0^o plies can be counted at both the left and right hand sides of the photograph, while four plies are evident at the center. Complete circumferential scans were made of several sections to determine the approximate percentage of excess plies due to gore overlap. A schematic of sample results are shown in figures 18(b) and indicate approximately 40 percent of the circumference was comprised of excess 0^o plies due to the overlap. Hence excessive axial stiffness behavior is inevitable. Although all of the remaining $[90/0_4/90]$ test specimens were not sectioned for similar microscopic examination, it appears from the structural behavior shown in figure 16 that gore overlap persisted

tnroughout the length of the column for all of these columns except C4A.

An estimate of the axial stiffness of the Gr/E portion of the test specimens based on measured load--end-shortening data may be determined by solving the following equation for $(Et_2)_{Gr/E}$:

$$\delta_{exp} = \frac{P}{\pi}\left\{\frac{\ell_1}{\bar{r}_o[(Et_1)_{Al} + (Et_2)_{Gr/E}]} + \frac{\ell_2}{(Et_2)_{Gr/E}\,(r_2 - r_1)}\ln\left(\frac{r_2}{r_1}\right)\right.$$

$$\left. + \frac{\ell_3}{\bar{r}_3[(Et_3)_{AL} + (Et_2)_{Gr/E}]} + \frac{\ell_4}{\bar{r}_4(Et_4)_{Al}} + \frac{\ell_5}{\bar{r}_5(Et_5)_{Al}}\right\} \qquad (3)$$

where δ_{exp} is the experimentally measured end-shortening under load P in the linear range of the data. Geometric quantities in equation (3) are defined in figure 19. Note that the short segments containing portions of the aluminum end fittings are treated as cylinders; hence the radii associated with these segments are barred quantities because they represent average values. As noted earlier, the second term on the right-hand side of equation (3) is derived in Appendix B and represents the end-shortening of the long, doubly tapered Gr/E portion of the

column. The values of $(Et_2)_{Gr/E}$ calculated from equation (2) are given in Table 5. Note that the $(Et_2)_{Gr/E}$ of the stiffer $(90/0_4/90)$ ply columns are 10 to 13 percent greater than the value for column C4A. Note also, in figure 16, that the asymptotic values of the load--end-shortening curves exhibited by these higher stiffness columns are also in the same percentage range above the buckling load of column C4A.

To further verify that gore overlap is responsible for this increased axial stiffness behavior exhibited by the columns, theoretical $(Et_2)_{Gr/E}$ is calculated using the method of reference 6 and plotted in figure 20 as a function of n, the number of zero degree plies in a $(90/0_n/90)$ type laminate. Figure 20 shows that $(Et)_{Gr/E}$ is essentially a linear function of n for this laminate and that the values computed by equation (3) for columns C3 and C4A agree well with theory. The slight discrepancies shown should be expected because, in the manufacturing process, the way the gores were cut and laid on the mandrel resulted in only a portion of each gore having the filaments aligned in the true zero degree direction. In figure 20 the intersection of the horizontal, dashed, curve (representing the axial stiffness of the stiffer columns) with the long dashed curve passing through the data points for columns C3 and C4A occurs at $n \approx 4.4$. Thus, the gore overlap is equivalent to an additional zero degree layer with a thickness of 40 percent of the original zero degree plies. This result tends to verify the speculation of the microscopic study given in figure 18 that gore overlap occurred over 40 percent of the cross-section everywhere along the length of the columns.

Elastically Supported Column Buckling Tests and Analysis

Results for various combinations of elastic boundary conditions applied to columns TA and TB are presented in Table 6. The blade-blade result most closely represents a column element between two cluster joints in a large space truss platform. As can be seen, the blade-blade restraint does closely approximate the simple support condition for which the cluster was designed showing less than a six percent increase over the result for the simply supported column. For the tripod test, however, a cluster joint was used only at the apex of the tripod; wall brackets being used at the three wall attachment points. This condition is best simulated by the bracket-blade column test and is seen to increase the buckling load of column TB by 21 percent above the simple support value. The bracket-bracket support condition was investigated with column TA and shows a 37 percent increase in buckling load over the simple support result. The brackets, however, were used solely for the laboratory test and have no application in an octetruss space structure.

Tripod Buckling Tests and Analysis

The tripod test buckling loads, F_{cr}, for load direction, $\vartheta = 0^{o}$, 30^{o}, and 60^{o} are given in Table 7. The strain gages on the column elements were monitored on an oscilloscope as a function of loading. Such load-strain curves are characteristically linear for slender straight columns until the buckling load is approached at which point the strains become large for small increments in the load. The asymptotic value of these curves was taken as the tripod buckling load. Two

buckling loads are given for the $\theta = 0^{o}$ load direction; one for the standard cluster joint and one for the modified cluster joint. (The standard cluster joint is very lightweight and has marginal strength capability in the loading plane to carry the applied force required to buckle the tripod for loads in the 30^{o} and 60^{o} directions; thus the heavier modified cluster joint was used). Although the modified cluster joint was heavier than the standard cluster joint, the additional stiffness at the tripod connections caused only a three percent increase in the 0^{o} buckling load over the value obtained when the standard cluster joint was used.

For a theoretical comparison, the buckling behavior of the tripod subject to loads at the apex, directed in a plane parallel to the base of the tripod was analyzed with the SPAR computer code (ref. 7). The primary function of this code is to perform stress, buckling, and vibrational analyses of linear finite-element systems. The finite element model is shown in figure 21. To simulate the taper, each half-column is divided into eight general beam-type firite elements which are numbered in the figure. Thus the tripod finite element model has a total of 49 joints (294 degrees of freedom before application of the boundary conditions). The aluminum blades (section no. 8, fig. 21) at one end of the tripod members are assumed to be interconnected to form the apex of the tripod at which point compatibility of displacements and rotations is enforced. The wall brackets used in the actual tests provided an elastic restraint at the base of the tripod. Detailed finite-element modeling of these brackets would be impractical; thus an alternate

method was used to analytically simulate the appropriate restraint. This method involved clamping the aluminum blades at the boundary and introducing an effective stiffness for the aluminum blades. The effective stiffness is determined by matching the buckling load for the bracket-blade support condition from the column test (see Table 6) to the result from a column buckling analysis of the identical finite element model of a column element of the tripod. The analytical buckling loads of the tripod are compared with test data in figure 22. The analytical buckling load for all values of load orientation is given by the solid line superimposed on a planform view of the tripod. Note that the most critical buckling load is predicted when only one of the tripod elements is in compression and the other two elements are under equal tensile loads ($\theta = 0^{o}$, 120^{o}, or 240^{o}). The maximum buckling load for the structure occurs at $\theta = 60^{o}$, 180^{o}, or 300^{o} when two of the elements are under equal compressive loads and the other element is in tension. The agreement with the test data at $\theta = 0^{o}$ is very good for the standard cluster joint (within three percent), thus the assumption of boundary restraints equal to the bracket-blade support arrangement from the column test appears valid. The modified cluster joint, however, does add some additional restraint to the tripod (exhibited by the separation of the two data points at $\theta = 0^{o}$) which was not included in the analysis. Neglecting this additional boundary restraint, however, does not account for the inconsistency of the test data which falls above theoretical predictions at $\theta = 0^{o}$ and 30^{o} but below theory at $\theta = 60^{o}$. A plausible explanation is that the elastic behavior of the cluster joint is not constant for

all orientations of the applied load, F. It is likely that the tendency for the cluster joint to remain a fixed node in space would be greater when two of its supporting elements are in tension ($\theta = 0^{o}$) than when only one supporting element is in tension ($\theta = 60^{o}$). This behavior, however, is peculiar to the tripod tests and would probably be inconsequential in a large space octetruss where the core members are lightly loaded, regardless of the loading direction in the face-plane of the truss. Tests of larger structural modules are necessary to address this question more accurately and appropriately.

CONCLUDING REMARKS

The buckling behavior of Gr/E nestable columns and a tripod arrangement of these columns including first generation joint concepts possessing features which are applicable to large-area truss-type space structures, has been experimentally investigated and compared with theory. From this investigation some insight into the joint designs as well as column structural behavior has been gained. Conclusions which can be drawn from this investigation are:

1. Column buckling loads are predictable with simple theory and are apparently insensitive to the interlocking center joint design used in this investigation.

2. Cyclic buckling does not appear to degrade the axial stiffness of the column nor the continuity of the center joint.

3. Axial stiffness of the columns may be significantly altered during fabrication unless care is taken to insure that gaps or overlaps between 0^{o} plies do not occur.

4. The cluster joint is held relatively stable in space by the tripod elements although there appears to be some variation in the restraint at the cluster joint as the load direction varies. Such behavior may be a result of the unusually heavy loading required to buckle the tripod and is expected to be insignificant in a large space octetrus where core members would be lightly loaded.

5. Tripod buckling loads are accurately predicted by a relatively simple finite element analysis when proper boundary restraint is taken into account.

APPENDIX A

DERIVATION OF EQUATION FOR BUCKLING FACTOR, m, FOR TAPERED TUBES

The Euler buckling load of a bar with continuously varying cross-section is given by (ref. 5)

$$P_{crit} = \frac{mEI_{max}}{\ell^2} \qquad A(1)$$

where E is Young's modulus of the material, ℓ is the length of the bar, and the factor, m, is a function of the ratio of I_{min} to I_{max}, the moments of inertia at the small and large ends of the bar, respectively. In the case of tapered tubes of constant thickness the cross-sectional moment of inertia varies according to the third power of the distance along the bar. Thus the method presented in reference 5 is applicable to the Gr/E nestable column elements studied in the present paper. The range covered in the table of m values presented in reference 5, however, does not include column geometries studied in the present paper, nor is the appropriate equation presented from which m can be calculated. The required equation is developed in this appendix.

The moment of inertia, I_x, at any axial station of a tapered tube can be expressed as

$$I_x = I_{min}\left(\frac{x}{a}\right)^3 \qquad A(2)$$

where I_{min} is the moment of inertia at the small end. The tube geometry and coordinate system are shown in figure 23. The differential equation of the deflection curve of the column under load p, then, is

$$EI_1 \left(\frac{x}{a}\right)^3 \frac{d^2y}{dx^2} = - Py \qquad A(3)$$

which may be written as

$$\frac{d^2y}{dx^2} + \frac{Pa^3}{EI_{min}x^3} y = 0 \qquad A(4)$$

Through a series of transformations given in reference 8, equation A(4) can be shown to be equivalent to Bessel's equation with a known solution. Thus the solution to equation A(4) may be written as

$$y = Ax^{1/2} J_{-1}\left[-2\left(\frac{Pa^3}{EI_{min}}\right)^{1/2} x^{-1/2}\right] + Bx^{1/2} Y_{-1}\left[-2\left(\frac{Pa^3}{EI_{min}}\right)^{1/2} x^{-1/2}\right] \qquad A(5)$$

where J_{-1} is a Bessel function of the first kind and Y_{-1} is a Bessel function of the second kind. The boundary conditions to be satisfied are

$$\left.\begin{aligned} y(a) &= 0 \\ \frac{dy\ (a + \ell/2)}{dx} &= 0 \end{aligned}\right\} \qquad A(6)$$

Making the substitutions

$$C^2 = 4\,\frac{Pa^3}{EI_{min}} \qquad A(7)$$

and

$$b = a + \frac{\ell}{2} \qquad A(8)$$

equations A(6) become

$$y(a) = 0 = Aa^{1/2}J_{-1}(Ca^{1/2}) + Ba^{1/2}\,Y_{-1}(Ca^{-1/2}) \qquad A(9)$$

and

$$\frac{dy(b)}{dx} = 0 = 1/2\ b^{-1/2}[AJ_{-1}(Cb^{-1/2}) + BY_{-1}\ (Cb^{-1/2})]$$

$$+ b^{1/2}\,[AJ'_{-1}(Cb^{-1/2}) - 1/2Cb^{-3/2} + BY'_{-1}(Cb^{-1/2}) - 1/2Cb^{-3/2}] \qquad A(10)$$

Using the following relations

$$
\left.
\begin{aligned}
J'_{-1}(z) &= -\frac{1}{z} J_{-1}(z) - J_0(z) = \frac{1}{z} J_1(z) - J_0(z) \\
Y'_{-1}(z) &= -\frac{1}{z} Y_{-1}(z) - Y_0(z) = \frac{1}{z} Y_1(z) - Y_0(z) \\
J_{-1}(z) &= - J_1(z) \\
Y_{-1}(z) &= - Y_1(z)
\end{aligned}
\right\} \qquad A(11)
$$

equations A(9) and A(10) may be written as

$$
\left.
\begin{aligned}
y(a) = 0 &= Aa^{1/2} J_1(Ca^{-1/2}) + Ba^{1/2} Y_1(Ca^{-1/2}) \\
\frac{dy(b)}{dx} = 0 &= A\left[-b^{-1/2}J_1(Cb^{-1/2}) + 1/2\ Cb^{-1}J_0(Cb^{-1/2})\right] \\
&\quad +B\left[-b^{-1/2}Y_1(Cb^{-1/2}) + 1/2\ Cb^{-1}Y_0(Cb^{-1/2})\right]
\end{aligned}
\right\} \qquad A(12)
$$

For a non-trivial solution for A and B to exist requires the determinant of the coefficients to vanish.

$$
\begin{vmatrix}
a^{1/2}J_1(Ca^{-1/2}) & a^{1/2}Y_1(Ca^{-1/2}) \\
-b^{-1/2}J_1(Cb^{-1/2}) + 1/2\ Cb^{-1}J_0(Cb^{-1/2}) & -b^{-1/2}Y_1(Cb^{-1/2}) + \frac{1}{2}Cb^{-1}Y_0(Cb^{-1/2})
\end{vmatrix} = 0 \qquad A(13)
$$

Recalling equations A(7) and A(1) and solving for C yields

$$C = 2\sqrt{\frac{ma^3}{\ell^2}\frac{I_{max}}{I_{min}}} \qquad A(14)$$

and from figure 23 it can be determined that

$$a = \frac{\ell r_{min}}{2(r_{max} - r_{min})} \qquad A(15)$$

Letting

$$\alpha = \left(\frac{I_{min}}{I_{max}}\right)^{1/3} = \frac{r_{min}}{r_{max}}$$

equations A(8), A(14) and A(15) can be written as

$$C = 2\sqrt{\frac{m\ell}{8\ (1-\alpha)^3}} \qquad A(16)$$

$$a = \frac{\ell\alpha}{2(1-\alpha)} \qquad A(17)$$

and

$$b = \frac{\ell}{2(1-\alpha)} \qquad A(18)$$

Substituting equations A(16), A(17) and A(18) into equation A(13) yields the desired relation

$$J_1\left(\sqrt{\frac{m}{\alpha(1-\alpha)^2}}\right)\left[\sqrt{\alpha}\,Y_1\left(\sqrt{\frac{m}{(1-\alpha)^2}}\right) - \frac{1}{2}\sqrt{\frac{m\alpha}{(1-\alpha)^2}}\,Y_0\left(\sqrt{\frac{m}{(1-\alpha)^2}}\right)\right]$$

$$-Y_1\left(\sqrt{\frac{m}{\alpha(1-\alpha)^2}}\right)\left[\sqrt{K}\,J_1\left(\sqrt{\frac{m}{(1-\alpha)^2}}\right) - \frac{1}{2}\sqrt{\frac{m\alpha}{(1-\alpha)^2}}\,J_0\left(\sqrt{\frac{m}{(1-\alpha)^2}}\right)\right] = 0 \qquad \text{A(19)}$$

The smallest non-zero value of m satisfying equation A(19) is the desired buckling factor to be used in equation A(1). Values of the factor m have been calculated and are plotted as a function of r_{min}/r_{max} in figure 17.

APPENDIX B

END-SHORTENING OF A TAPERED TUBE

An expression for the total end-shortening of a doubly-tapered tube (such as formed from two nestable half-columns) under a compressive load, P, can be derived from Hook's law,

$$\sigma = E\varepsilon \qquad B(1)$$

and the definitions of simple stress

$$\sigma = \frac{P}{\tilde{A}} \qquad B(2)$$

and average strain

$$\varepsilon = \frac{\delta}{L} \qquad B(3)$$

For a tapered tube of constant thickness t, the area, $\tilde{A}$, is a function of x, the axial coordinate; thus these equations apply only for a differential length over which the cross-section is constant. By substituting equations B(1) and B(2) into the differential form of equation B(3), the end shortening over a differential length dx can be written as

$$d\delta = \frac{P dx}{\tilde{f} E} \qquad B(4)$$

The total column end-shortening is twice the integral of these infinitesimal end-shortenings over the range of x from zero to ℓ (column half-length) and may be expressed as

$$\delta = \frac{P}{\pi E t} \int_0^{\ell} \frac{dx}{r(x)} \qquad B(5)$$

where $r(x)$ is the radius of the tube. Letting r_{min} be the radius of the small end of a half-tube and r_{max} be the radius of the large end, the radius at any point is

$$r = \frac{r_{max} - r_{min}}{\ell} x + r_{min} \quad (0 \leq x \leq \ell) \qquad B(6)$$

Substituting equation B(6) into equation B(5) and integrating yields the expression for end-shortening of a doubly tapered, symmetric column of length $L = 2\ell$.

$$\delta = \frac{PL}{2\pi E t (r_{max} - r_{min})} \ln \left| \frac{r_{max}}{r_{min}} \right| \qquad B(7)$$

An axial stiffness measure, Et, of the doubly-tapered column can be determined from equation B(7), which is

$$Et = \left(\frac{P}{\delta}\right) \frac{L}{2\pi(r_{max} - r_{min})} \ln \left|\frac{r_{max}}{r_{min}}\right| \qquad B(8)$$

where $\left(\frac{P}{\delta}\right)$ is determined experimentally.

REFERENCES

1. Borrego, John: Space Grid Structures, Skeletal Frameworks and Stressed-Skin System. The MIT Press, 1972. LOC cat. card no. 67-27342.

2. Mikulas, Martin M., Jr.; Bush, Harold G.; and Card, Michael F.: Structural Stiffness, Strength and Dynamic Characteristics of Large Tetrahedral Space Truss Structures. NASA TM X-74001, March 1977.

3. Bush, Harold G.; and Mikulas, Martin M., Jr.: A Nestable Tapered Column Concept for Large Space Structures. NASA TM X-73927, July 1976.

4. Bush, Harold G.; Mikulas, Martin M.,Jr.; and Heard, Walter L., Jr.: Some Design Considerations for Large Space Structures. AIAA Paper No. 77-395, AIAA/ASME 18th Structures, Structural Dynamics, and Materials Conference, San Diego, CA, March 21-23, 1977.

5. Timoshenko, Stephen P.; and Gere, James M.: Theory of Elastic Stability. 2nd Edition, McGraw Hill Book Company, 1961.

6. Muha, T. J.: Users Manual for the Laminate Point Stress Analysis Computer Program SQ5 as Revised by AFDL/FBC. AFFDL-TM-74-107 FBC, Jul, 1974.

7. Whetstone, W. D.: SPAR Structural Analysis System Reference Manual, System Level II, vol 1, Program Execution. NASA CR 145098-1, February 1977.

8. V. Karman, Theodore and Biot, Maurice A.: Mathematical Methods in Engineering. McGraw-Hill Book Company, 1940.

Table 1.- Test Specimen Specifications

Specimen Designation	Ply Layup	Mass kg	Length, m		
			$\bar{\ell}_1$	$\bar{\ell}_2$	$\bar{L} = \bar{\ell}_1 + \bar{\ell}_2$
C3	$90/0_3/90$	1.402*	2.599	2.599	5.198
C4A	$90/0_4/90$	1.656*	2.599	2.599	5.198
C4B	↓	1.853†	2.600	2.601	5.201
C4C	↓	1.847†	2.600	2.601	5.201
TA	↓	1.896†	2.600	2.600	5.200
TB	↓	1.854†	2.600	2.601	5.201
TC	↓	1.903†	2.601	2.601	5.202

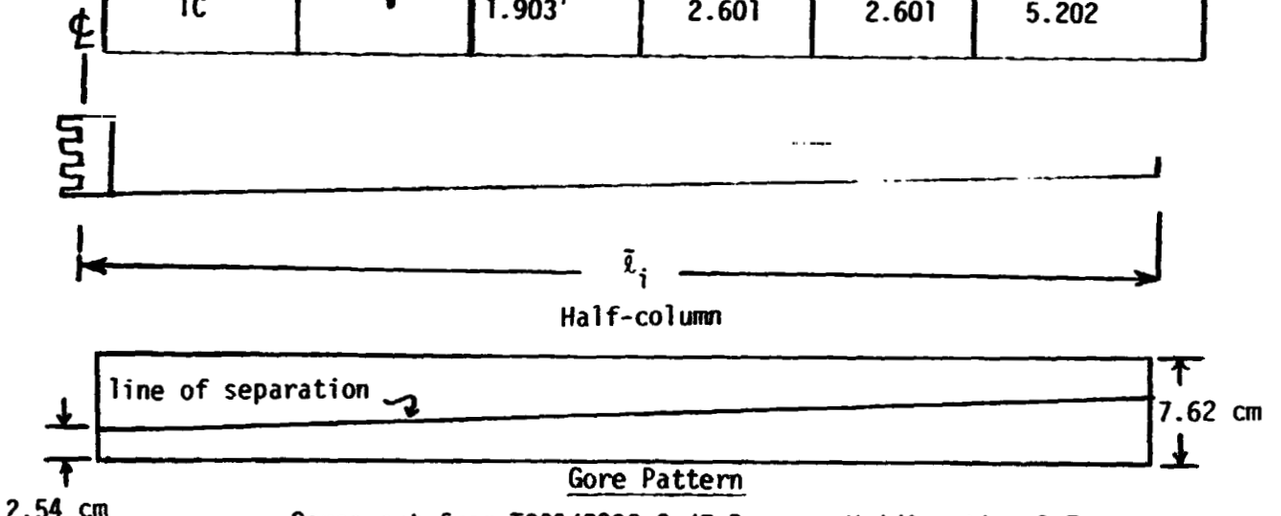

Gores cut from T300/5208 Gr/E Prepreg Unidirectional Tape

*Mass includes one full center joint (fig. 2), two threaded studs and two stud adapters (figure 5).

†Mass includes one full center joint (fig. 2) and two clevis receiver sleeves (figure 3).

Table 2. - Material Properties for
T300/5208 Gr/E Unidirectional
Prepreg Tape

$E_1 = 131\ GP_a$

$E_2 = 10.9\ GP_a$

$G = 5.24\ GP_a$

$\nu_1 = .32$

Table 3. - Masses of Joint Components

Hardware	Average Mass, gm
$\frac{1}{2}$ Center Joint (fig. 2)	80.7
Snap-In Clevis (fig. 3)	62.1
Clevis receiver sleeve (fig. 3)	24.9
Snap Ring (fig. 3)	4.1
Cluster Joint (fig. 3)	60.5
Threaded Stud (fig. 5) (Used in Columns C3 & C4A)	30.8

Table 4.- Column Buckling Loads

(a) Theoretical Buckling loads, $P_{crit} = \frac{m\pi Et r_{max}^3}{(L)^2}$

Test Specimen	Simple Support Length, L cm	Buckling Factor, m	Radius r_{max} cm	Et (Exp.Col.) MN/m	P_{crit} (Theory) kN
C3	530.9	5.300	5.108	54.73	4.309
C4A	530.9	5.300	5.115	74.64	5.901
C4B	532.6	5.284	↓	83.39	6.531
C4C	532.6	↓	↓	83.46	6.536
TA	532.5	↓	↓	84.24	6.600
TB	532.6	↓	↓	83.11	6.509
TC	532.7	↓	↓	84.04	6.579

(b) Experimental Buckling Loads and Comparison with Theory

Test Specimen	$P_{crit, Exp.}$ kN	$\frac{P_{crit,Exp.}}{P_{crit,Theory}*}$
C3	4.204	.98
C4A	5.707	.97
C4B	6.361	.97
C4C	6.325	.97
TA	6.490	.98
TB	6.370	.98
TC	6.497	.99

*From Table 4(a).

Table 5. - Axial Stiffnesses of Gr/E Laminates Determined From Measured Deflections Using Equation (3)

Test Specimen	$(Et)_{Gr/E}$ MN/m	Nominal Layup
C3	53.33	$90/0_3/90$
C4A	72.52	$90/0_4/90$
C4B	80.86	↓ Gore Overlap
C4C	80.01	
TA	81.89	
TB	80.86	
TC	80.88	

Table 6. - Influence of End Supports on Column Buckling Load

Test Specimen	*Support Conditions	Experimental Buckling Load P_{cr}, kN	$\frac{P_{cr}}{(P_{cr})_{ss}}$
TA	Simple Supports	6.490	1.00
TB		6.370	1.00
TB	Blade-Blade	6.752	1.06
TB	Bracket-Blade	7.722	1.21
TA	Bracket-Bracket	8.910	1.37

*See figure 13 for description of blade and bracket support conditions.

Table 7. - Tripod Experimental Buckling Loads

Load Direction $\theta°$	*Cluster Joint	Buckling Load, F_{cr} kN
0	Standard	6.85
0	Modified	7.07
30	Modified	8.36
60	Modified	12.65

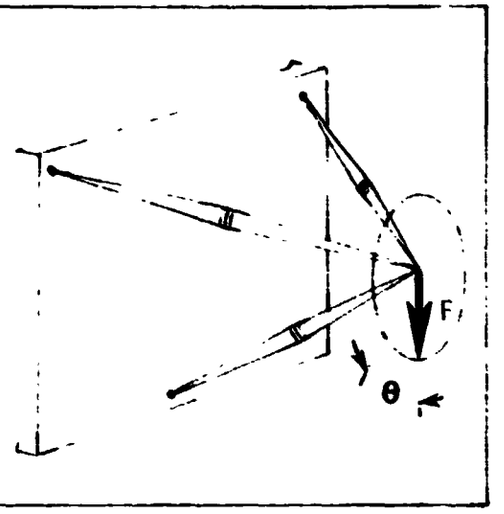

*See figure 15.

ORIGINAL PAGE
OF POOR QUALITY

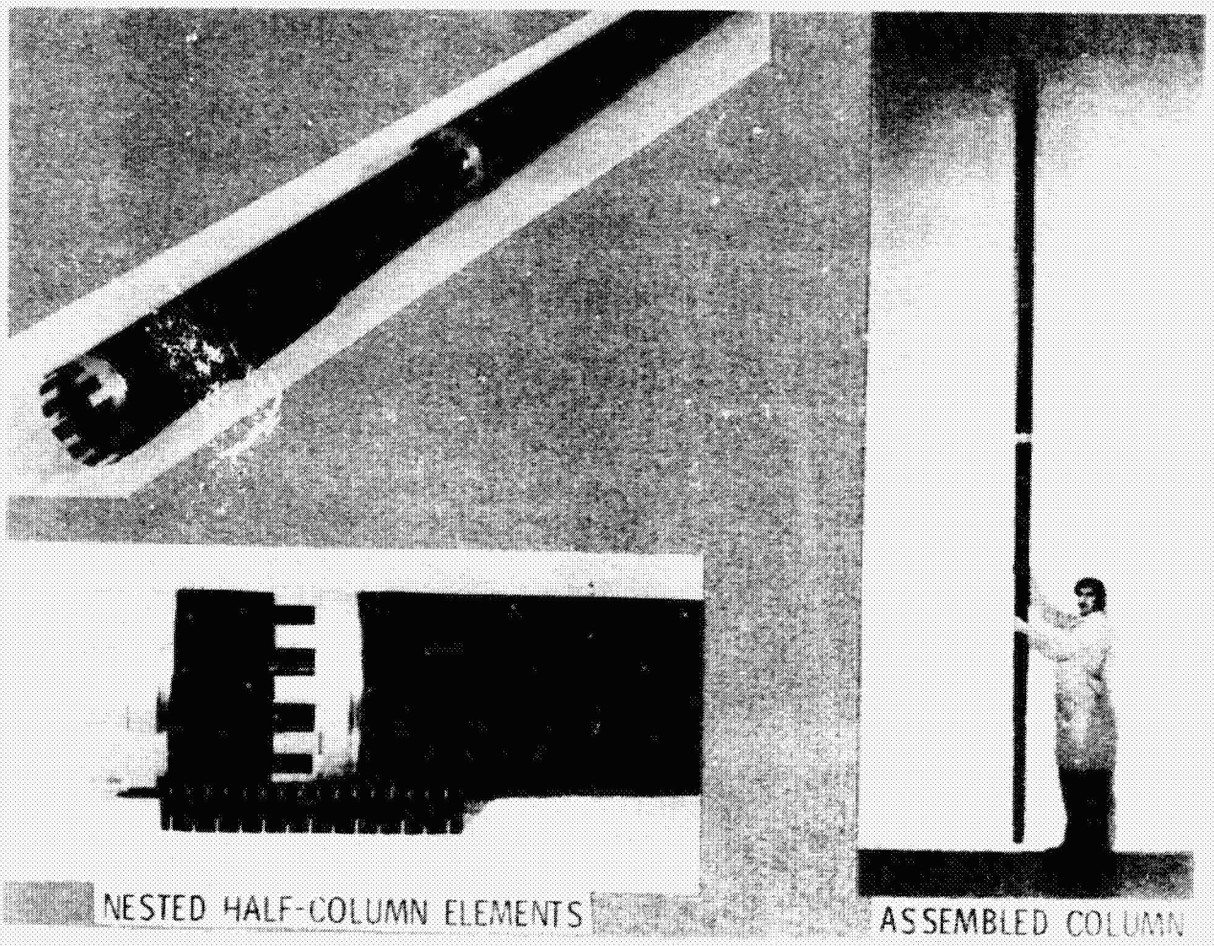

Figure 1.- Nestable column concept.

ORIGINAL PAGE IS
OF POOR QUALITY

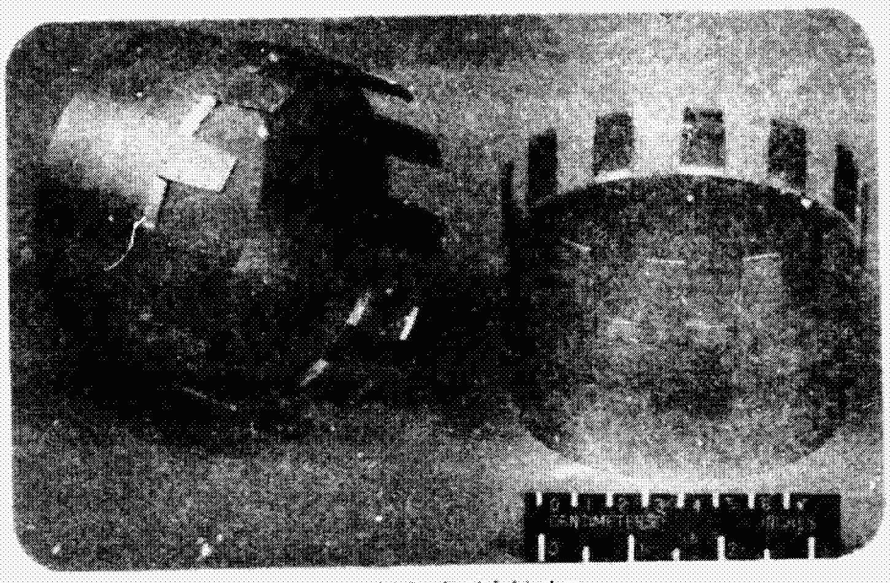

(a) Center joint halves

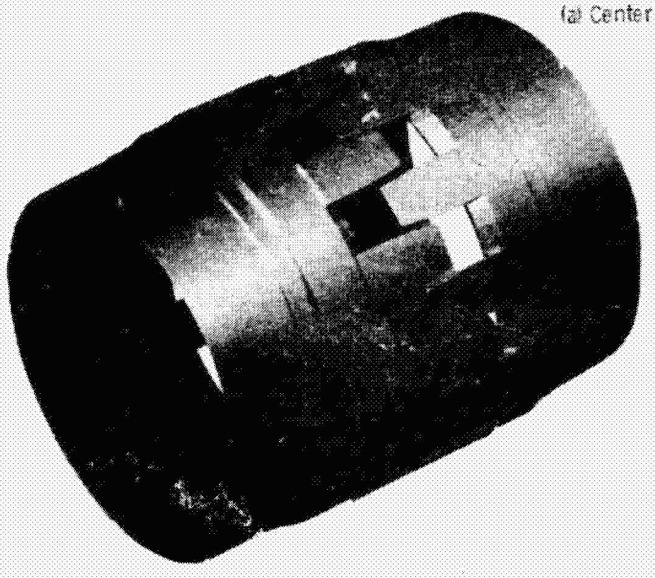

(b) Aligned for locking

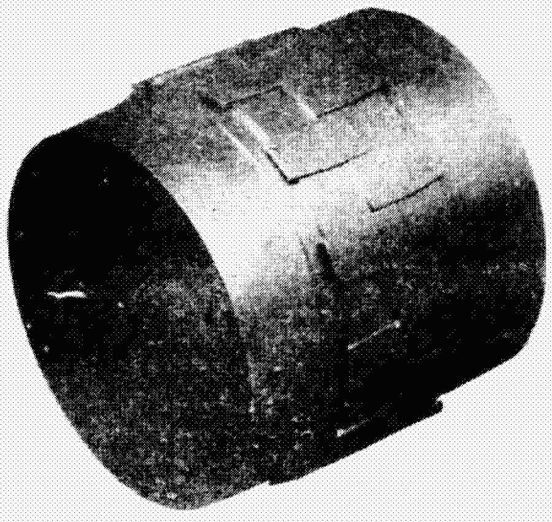

(c) Fully locked

Figure 2.- Center joint for nestable column.

ORIGINAL PAGE
OF POOR QUALITY

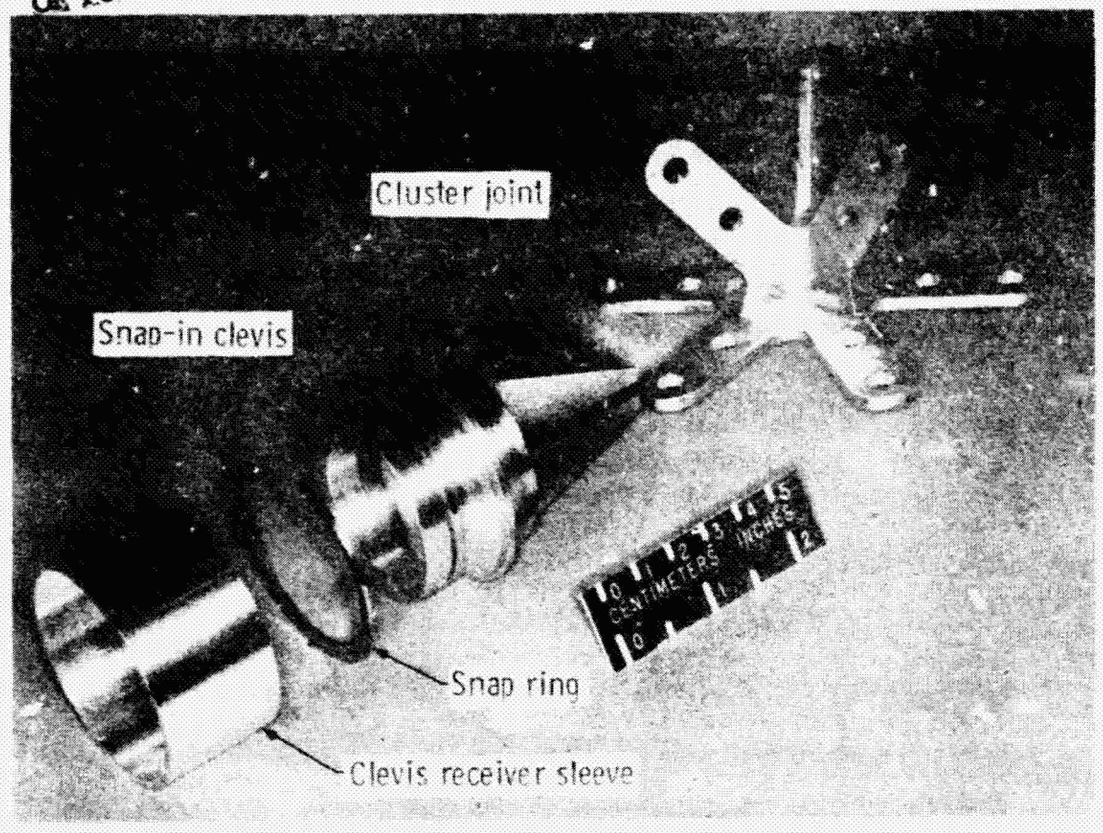

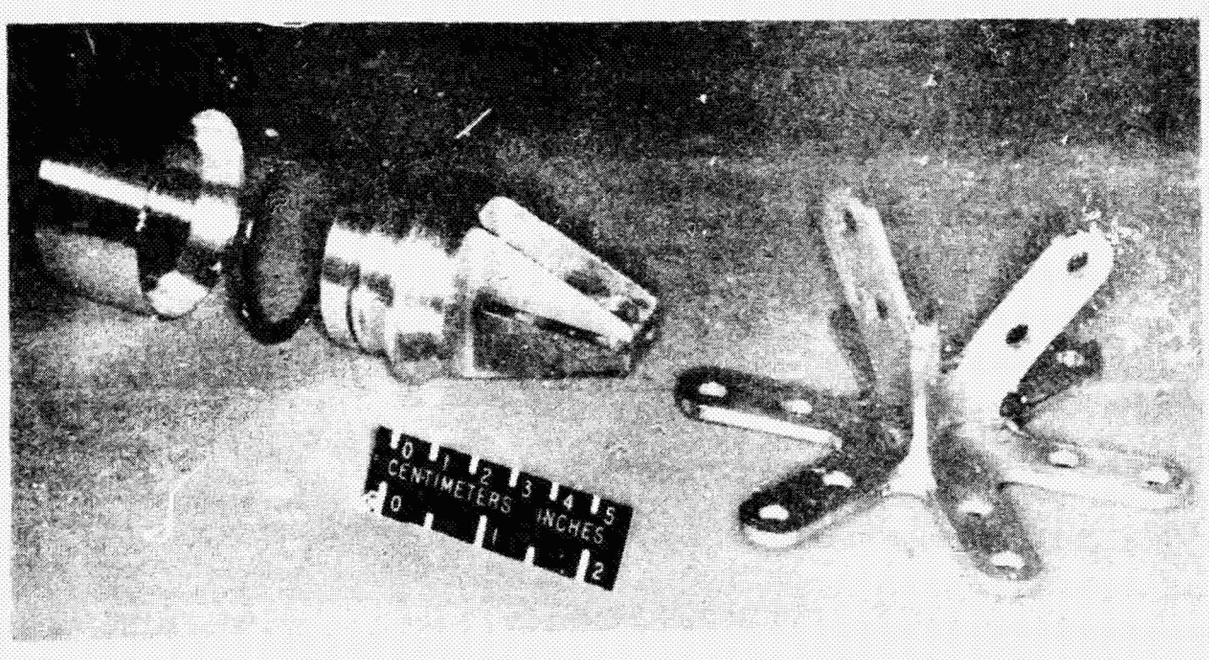

Figure 3.- Column end joint to cluster joint arrangement.

ORIGINAL PAGE IS
OF POOR QUALITY

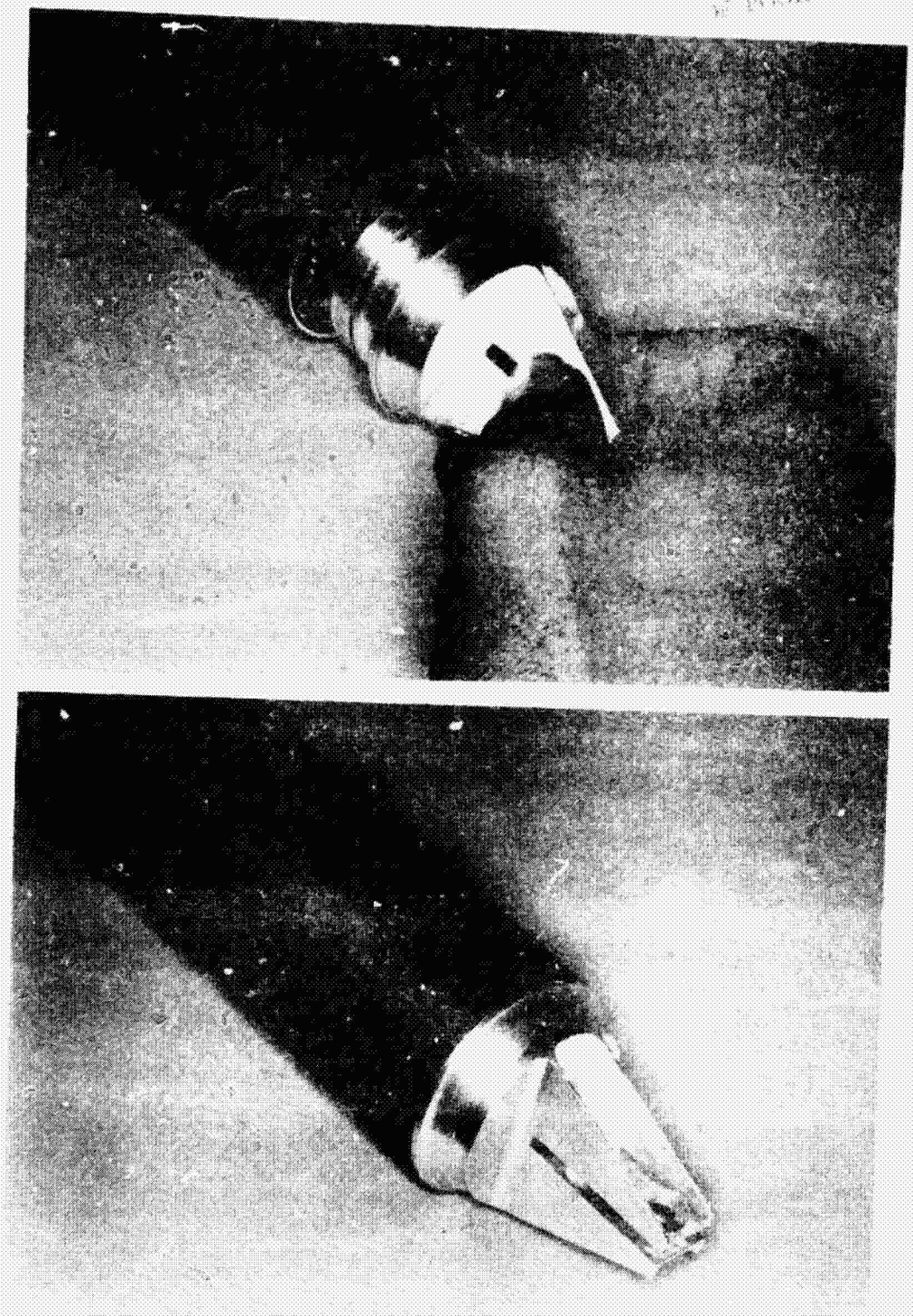

Figure 4.- Clevis end joints for nestable columns.

ORIGINAL PAGE IS
OF POOR QUALITY

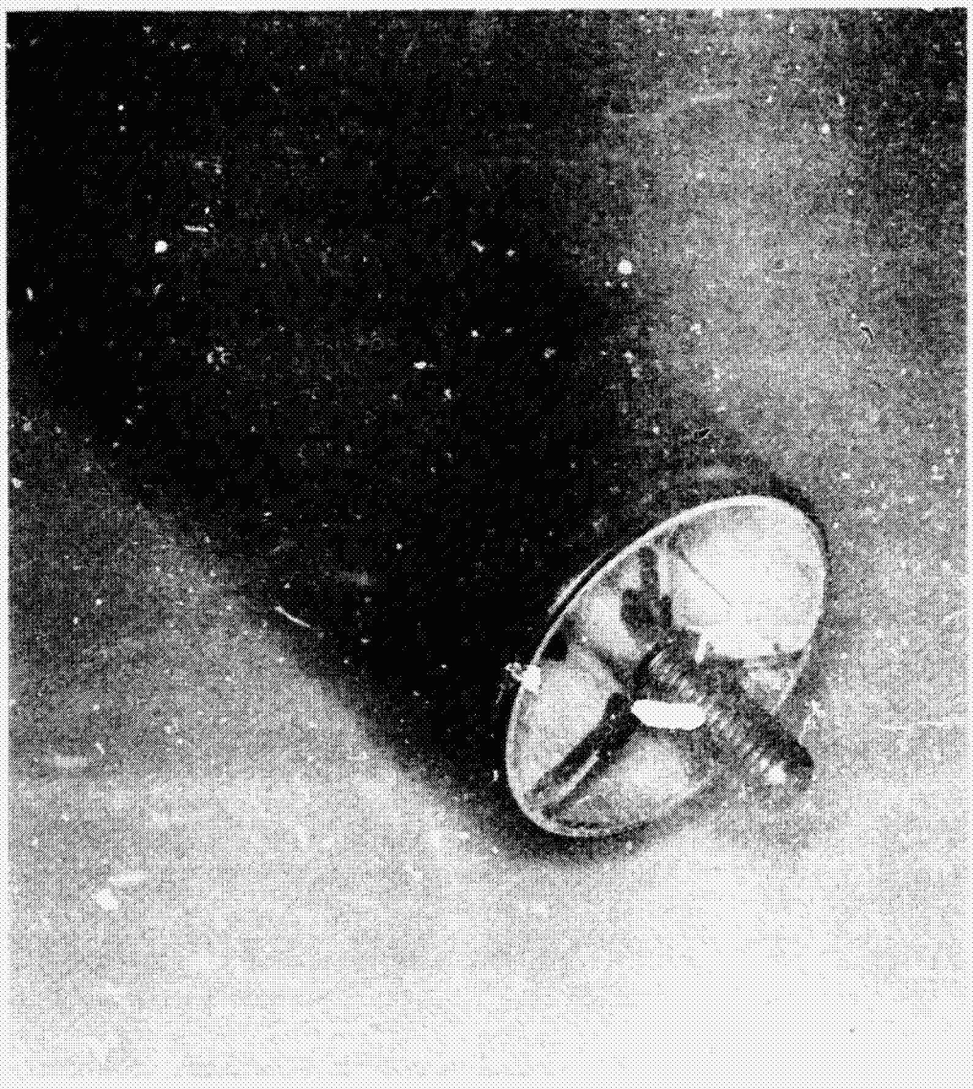

Figure 5.- Typical end fitting for columns C3 and C4A.

ORIGINAL PAGE
OF POOR QUA

Figure 6.- Method of assembly of column clevis joint to cluster joint.

ORIGINAL PAGE IS
OF POOR QUALITY

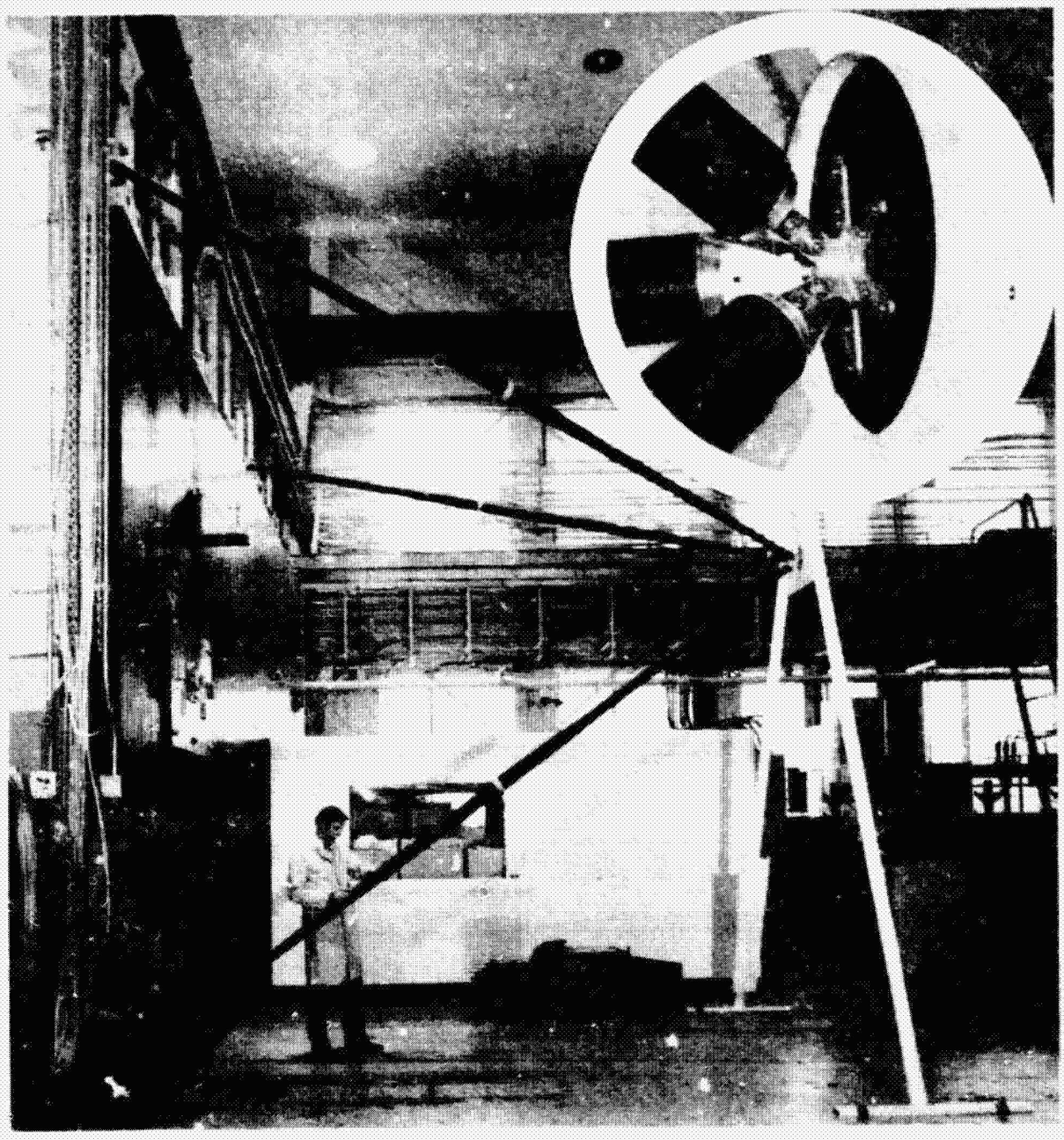

Figure 7.- Cluster joint installed at apex of tripod.

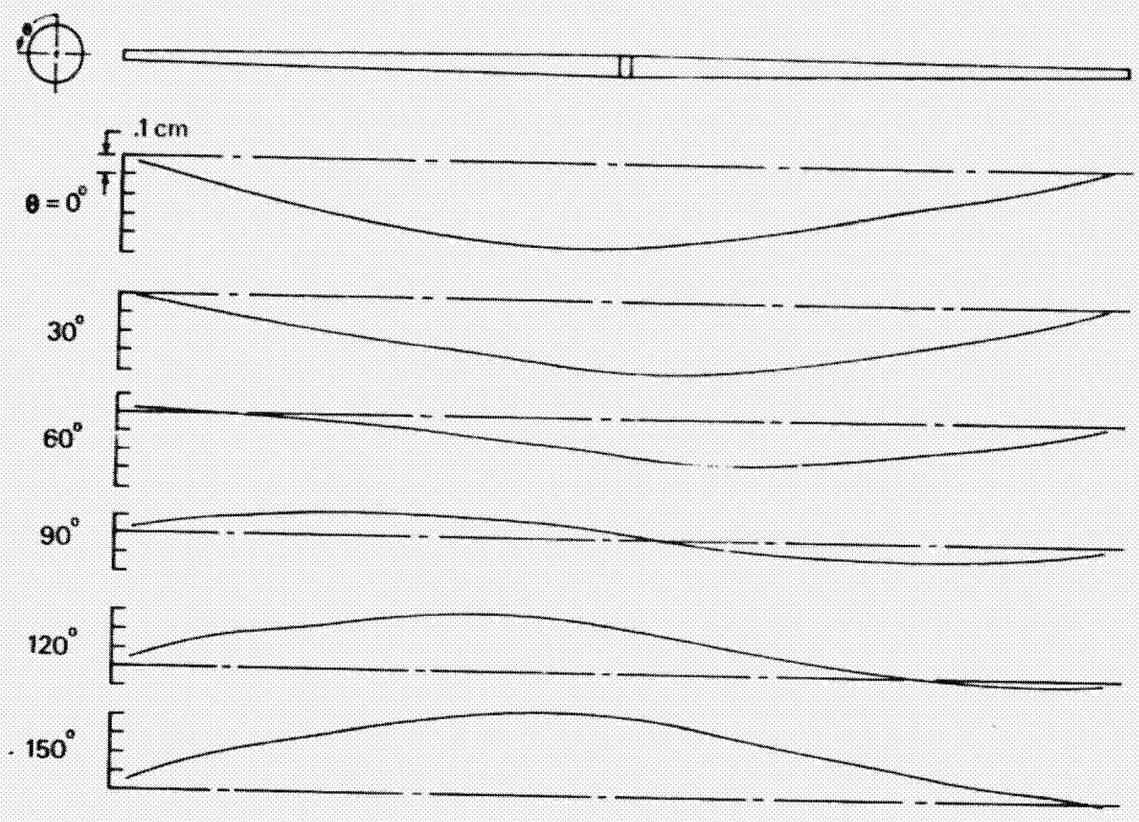

(a) Column C3

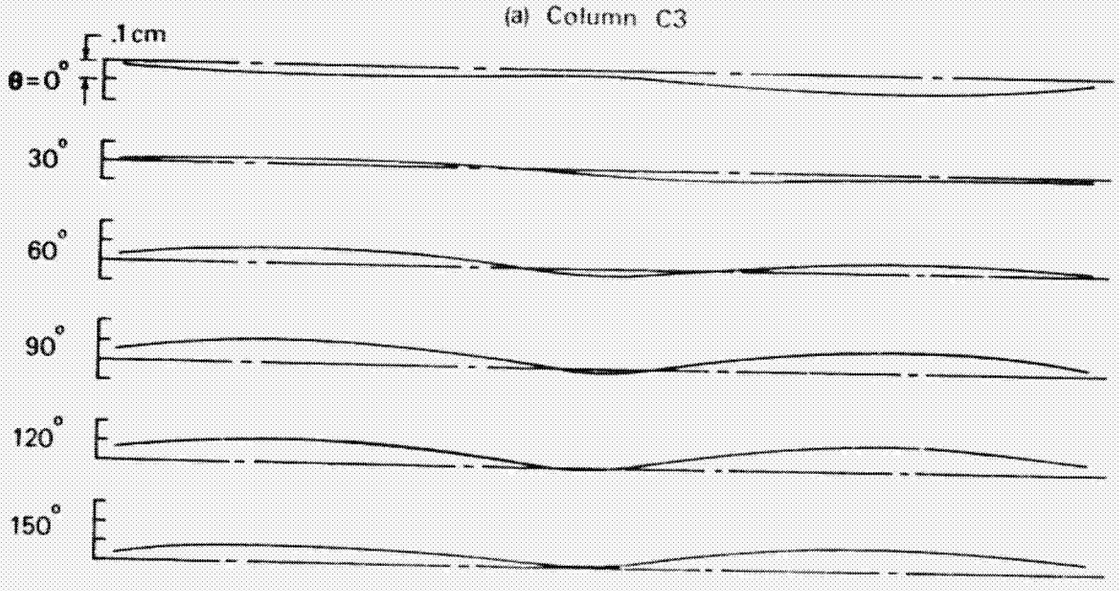

(b) Column C4A

Figure 8.- Measured initial imperfection in column straightness.

ORIGINAL PAGE
OF POOR QUALITY

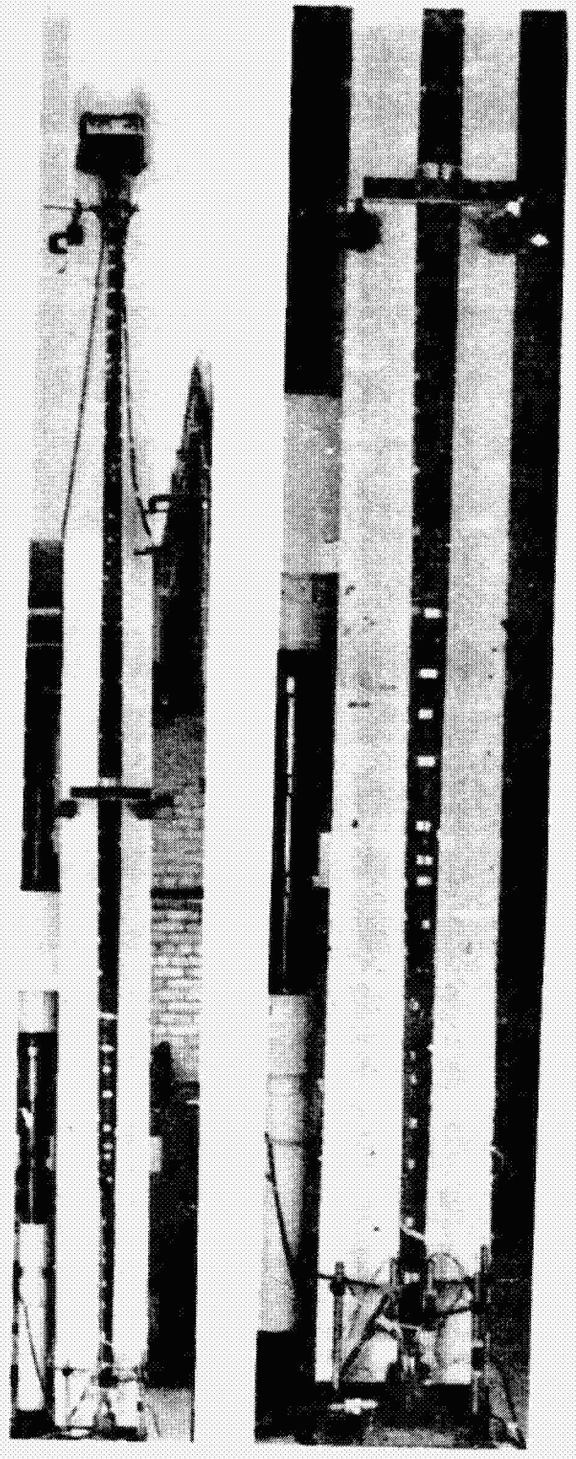

Figure 9.- Column test specimen mounted in loading fixture.

ORIGINAL PAGE IS
OF POOR QUALITY

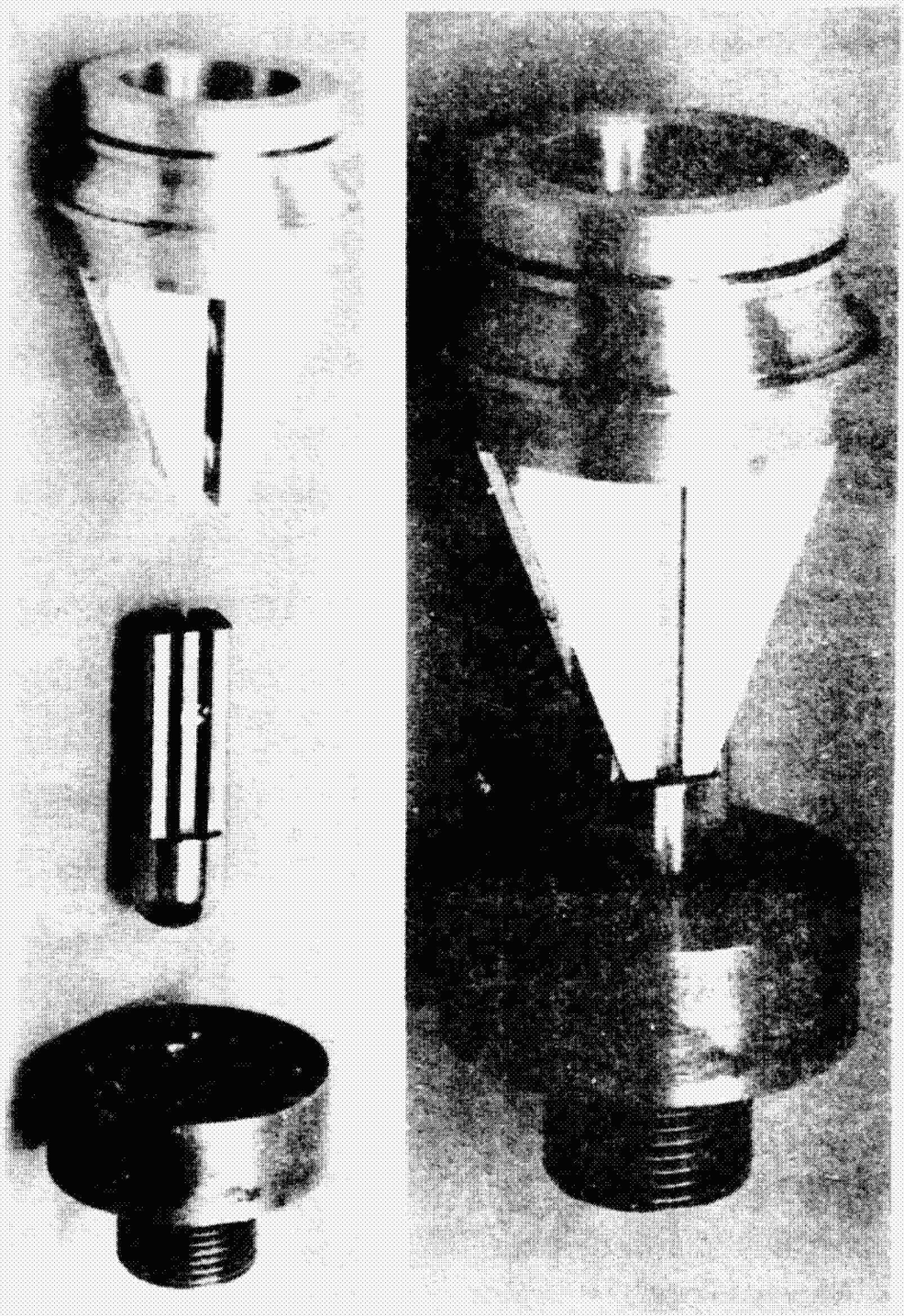

Figure 10.- Ball and cup end fittings for column tests.

ORIGINAL PAGE IS
OF POOR QUALITY

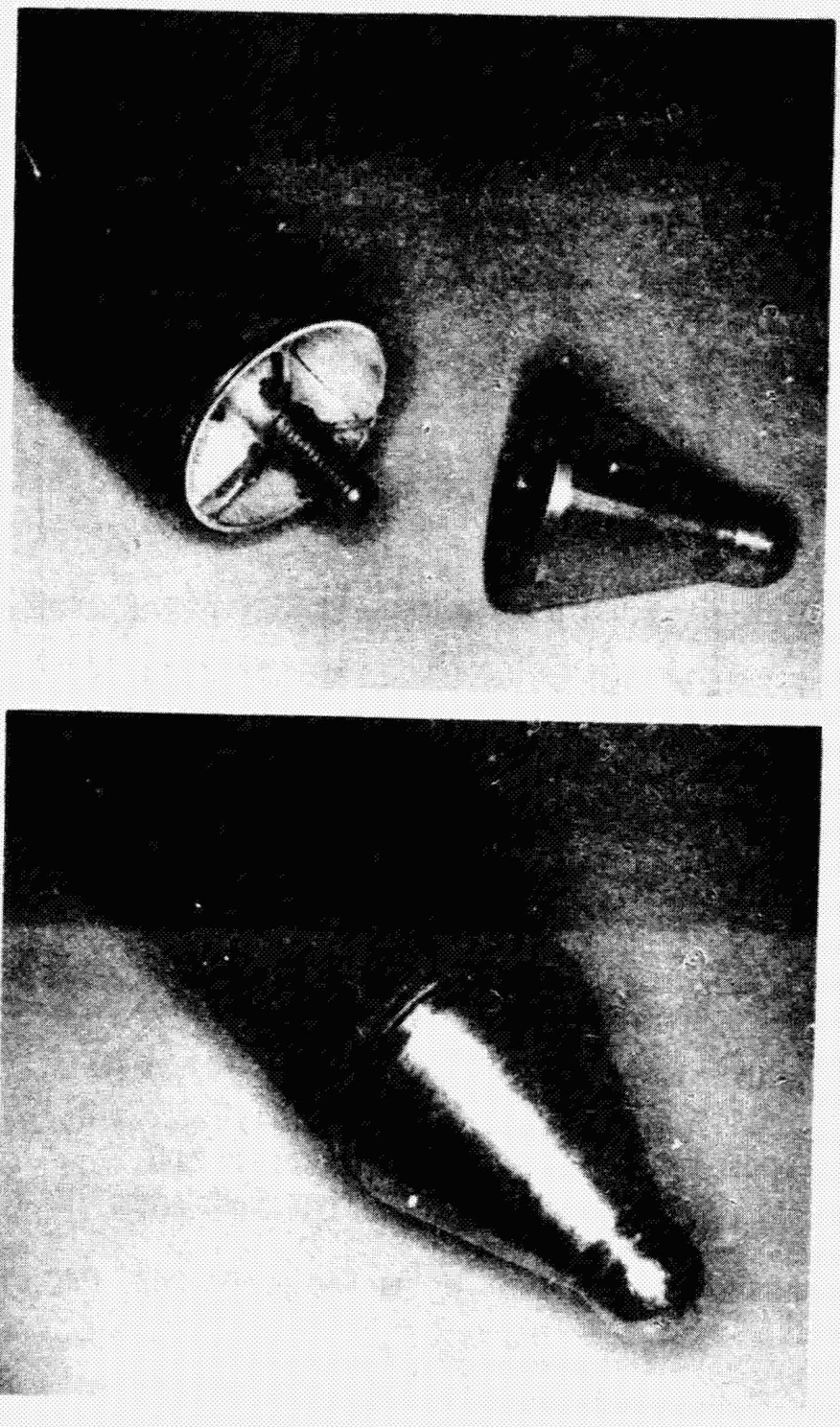

Figure 11.- Ball fittings for columns C3 and C4A.

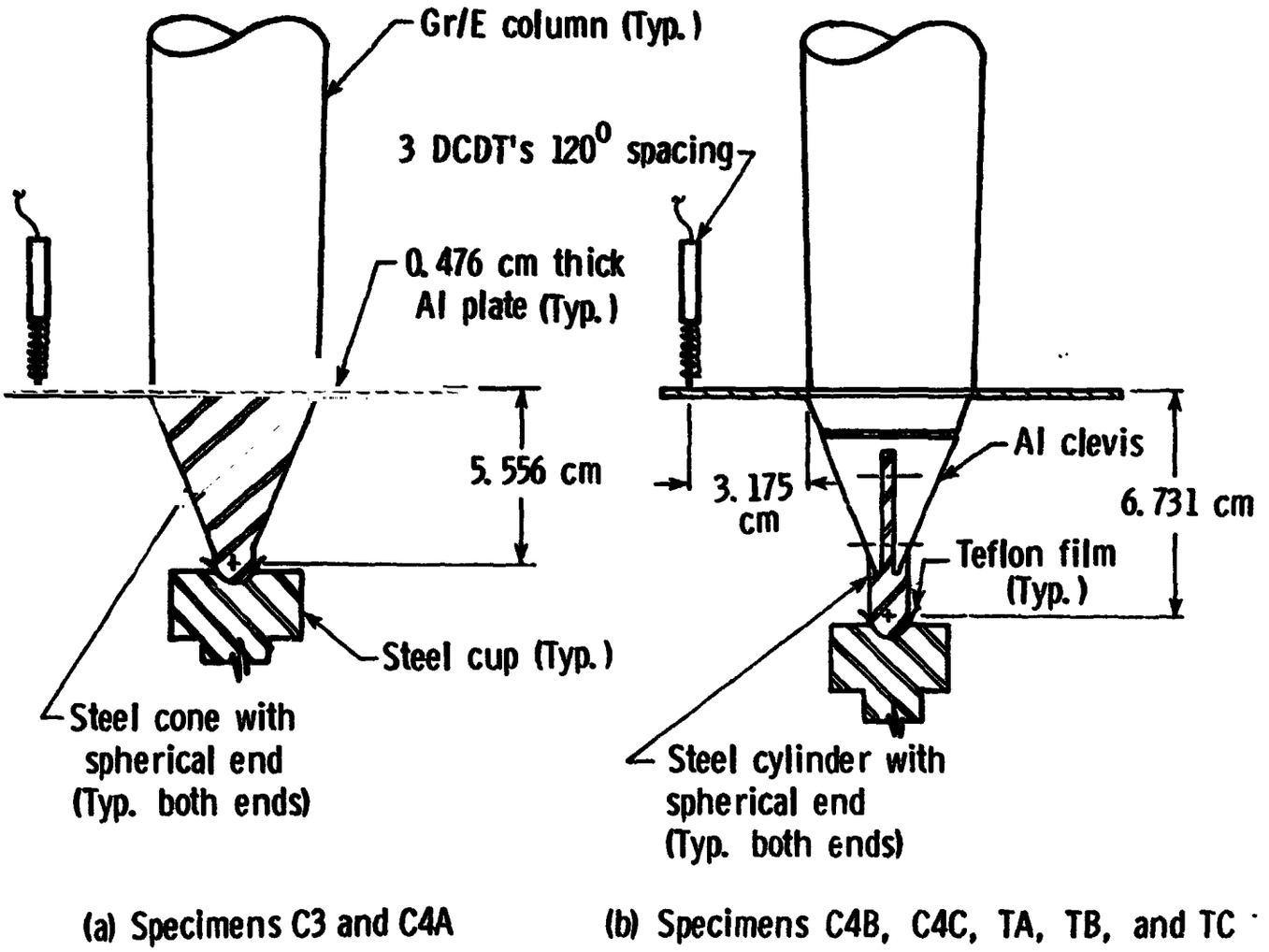

Figure 12.- End support arrangement and location of deflection measuring instrumentation (DCDT's).

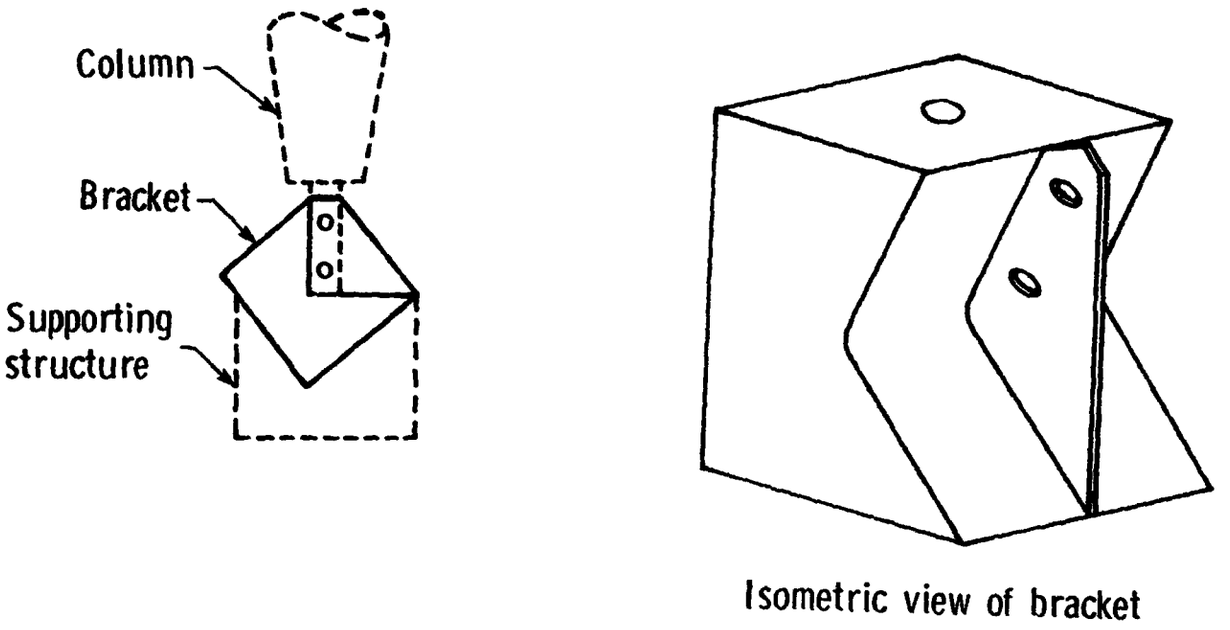

(a) Bracket

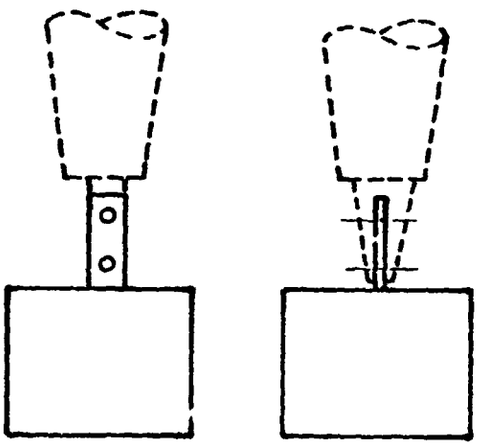

(b) Blade

Figure 13.- Bracket and blade end supports for elastically supported column tests.

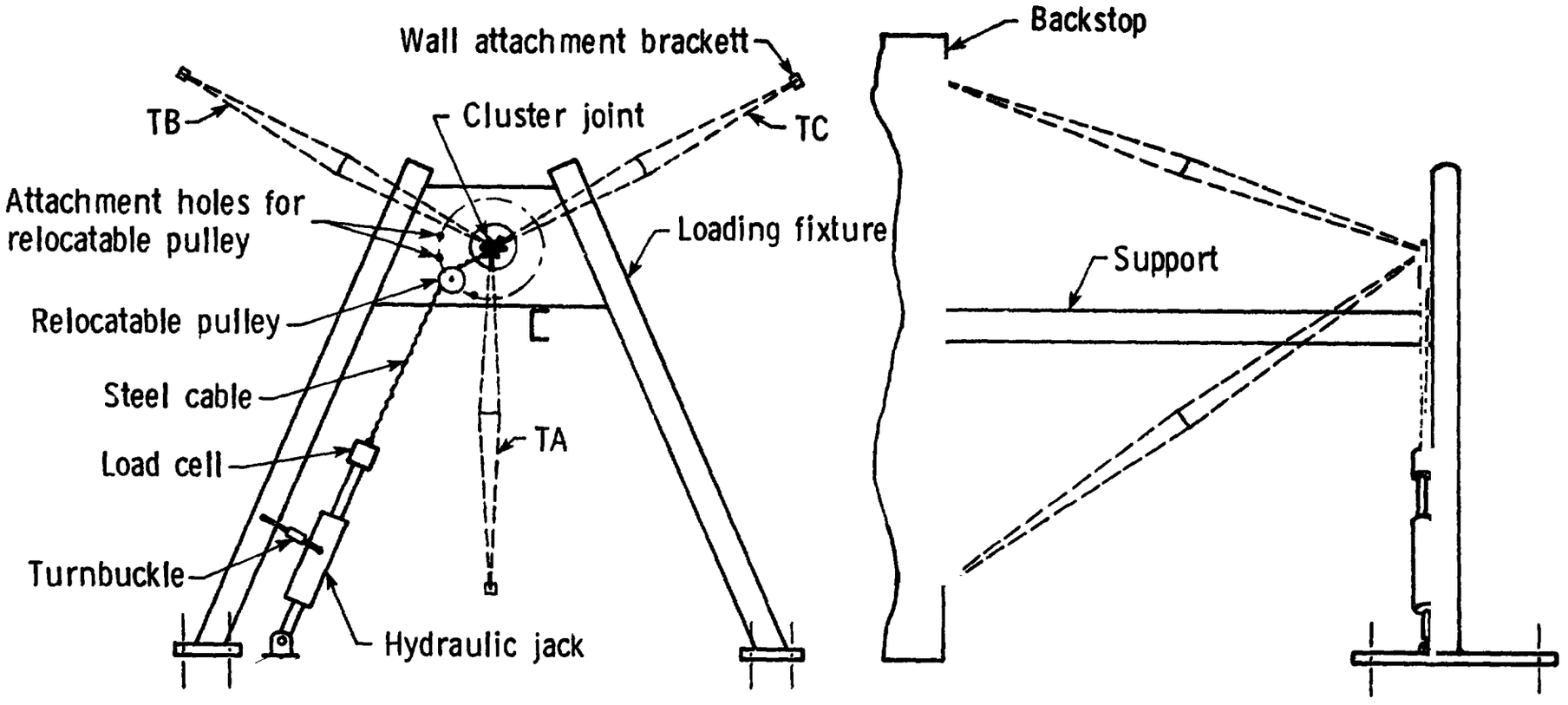

Figure 14.- Loading fixture for tripod buckling tests.

ORIGINAL PAGE IS
OF POOR QUALITY

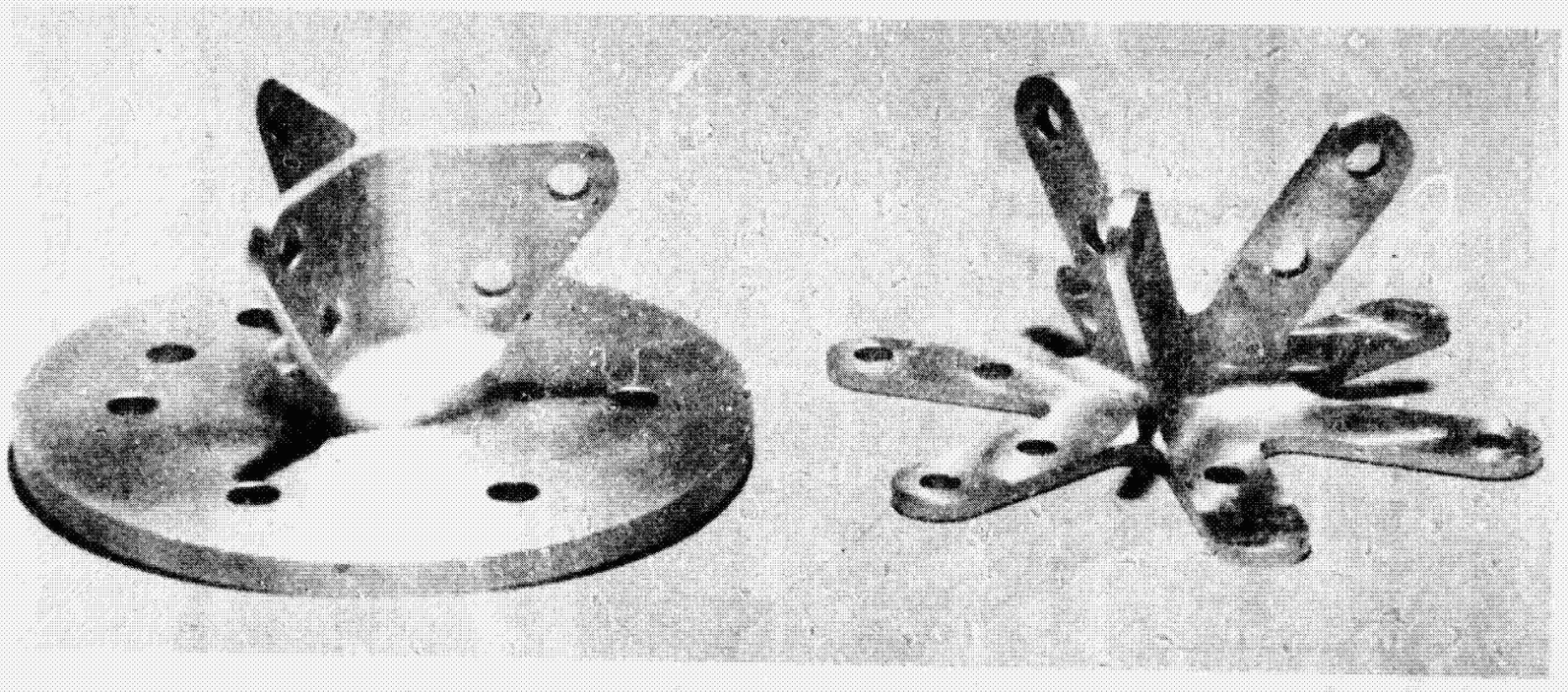

(a) Modified cluster joint

(b) Standard cluster joint

Figure 15.- Cluster joints used in tripod tests.

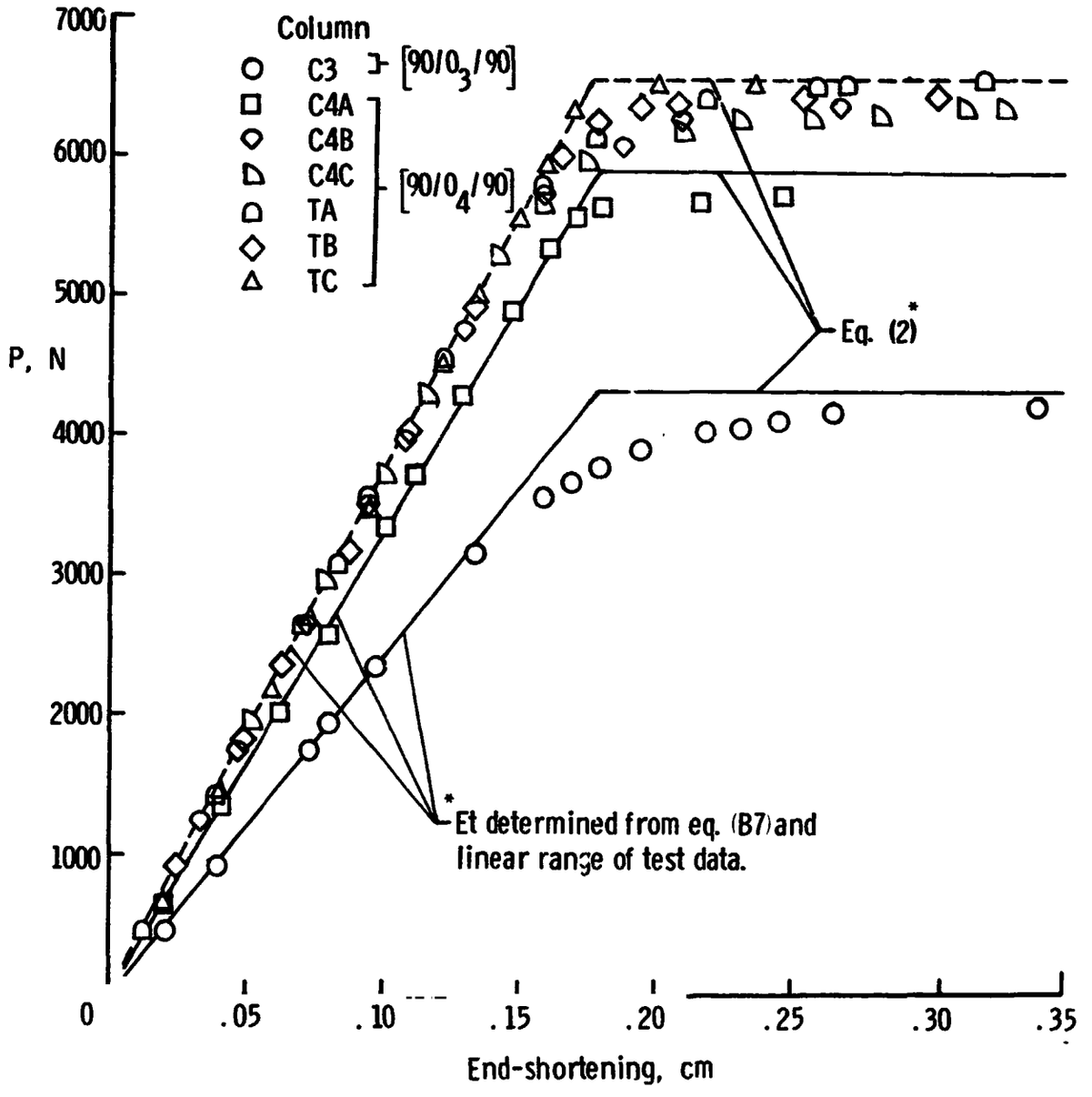

Figure 16.- Load--end-shortening data from column tests.

ORIGINAL PAGE IS
OF POOR QUALITY

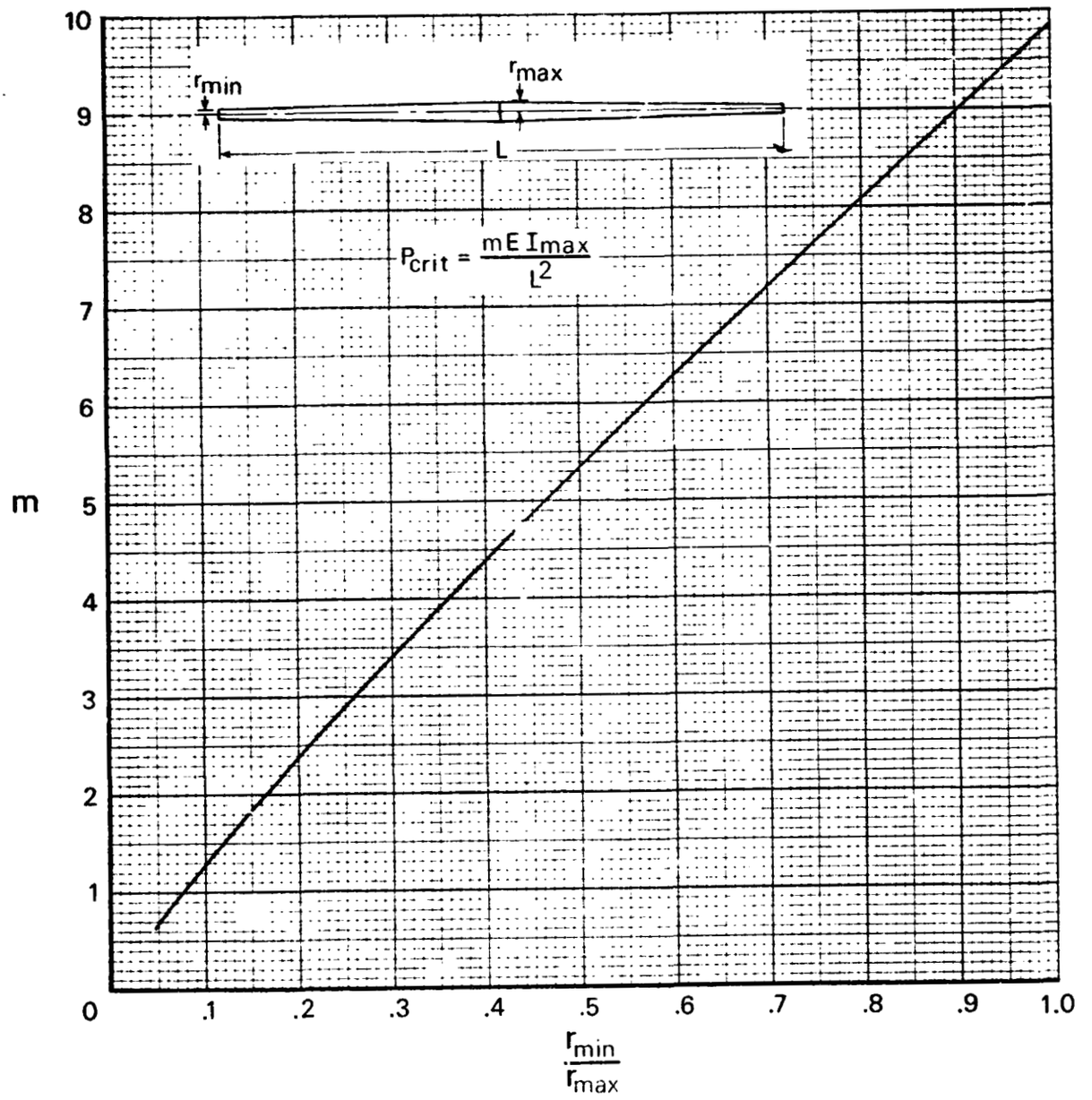

Figure 17.- Buckling factor, m, as a function of taper ratio for a doubly tapered tube.

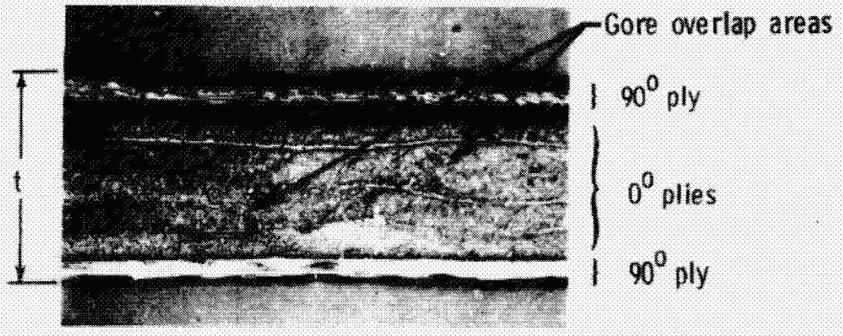

(a) Microscopic view of sample section of column wall.

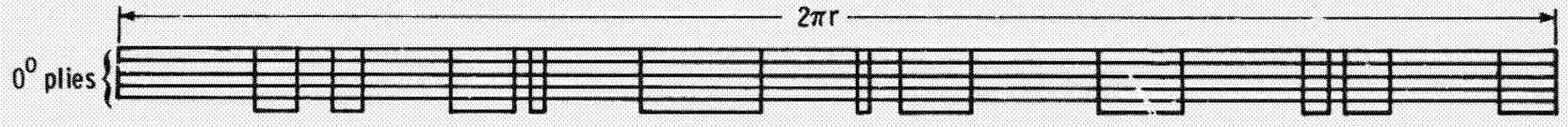

(b) Schematic of circumferential scan of column wall section showing approximately 40% of circumference with gore overlap.

Figure 18.- Sample results of microscopic studies of cross-sections of columns C4B, C4C, TA, TB, and TC.

ORIGINAL PAGE IS
OF POOR QUALITY

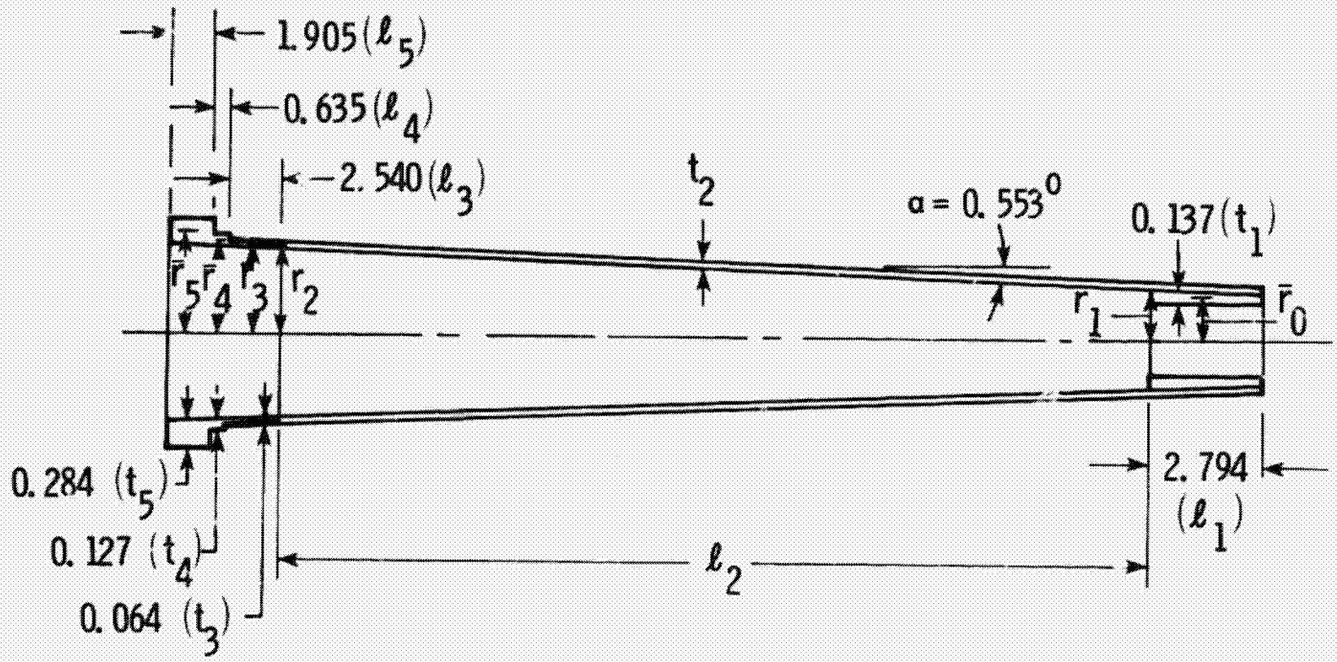

Column	Dimensions, cm							
	t_2	ℓ_2	$\bar{r}_0$	r_1	r_2	$\bar{r}_3$	$\bar{r}_4$	$\bar{r}_5$
C3	0.057	259.9	2.545	2.627	5.060	5.040	5.122	5.213
C4A	0.071	↓	2.552	2.634	5.067	5.047		
C4B		260.0	2.550	2.632				
C4C			↓	↓				
TA			2.551	2.633				
TB			2.550	2.632				
TC		260.1	↓	↓				

Figure 19.- Geometric quantities to be used in equation (3) for calculating axial stiffnesses from measured end-shortening data.

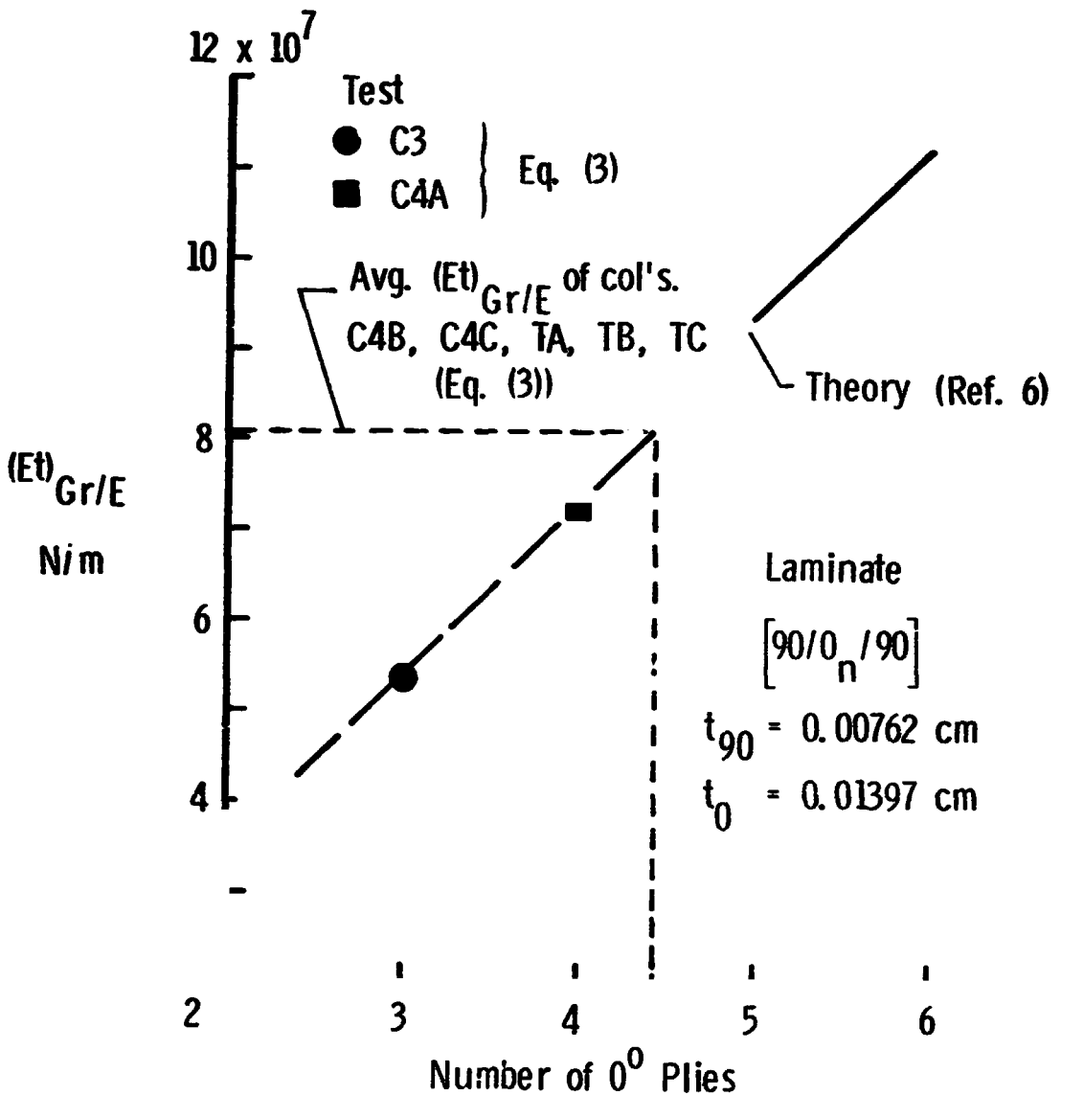

Figure 20.- Column axial stiffness parameter as a function of the number of 0^{o} plies.

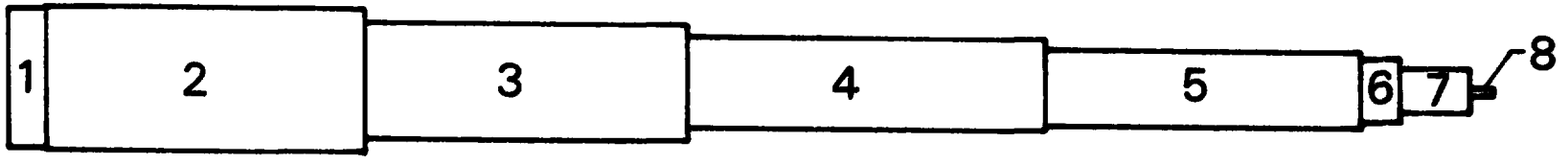

Section	Length	Area	Ix	Iy	J	Mat'l	E	μ	ρ
	cm	cm^2	cm^4	cm^4	cm^4		GPa		kg/m^3
1	2.540	9.922	133.319	133.319	266.638	Al	73.77	0.33	2.796
2	64.389	2.292	30.135	30.135	60.270	Gr/E	133.90	0.09516	1.522
3	64.389	1.851	15.879	15.879	31.758	Gr/E	133.90	0.09516	1.522
4	64.389	1.574	9.756	9.756	19.512	Gr/E	133.90	0.09516	1.522
5	61.595	1.277	5.215	5.215	10.430	Gr/E	133.90	0.09516	1.522
6	2.794	4.316	12.716	12.716	25.432	Gr/E+Al	81.21	0.29	2.436
7	5.080	0.862	0.524	1.224	0.003	Al	73.77	0.33	2.796
8	1.270	0.484	0.004	0.094	0.014	Al	73.77	0.33	2.796

Figure 21.- Finite element model of tripod.

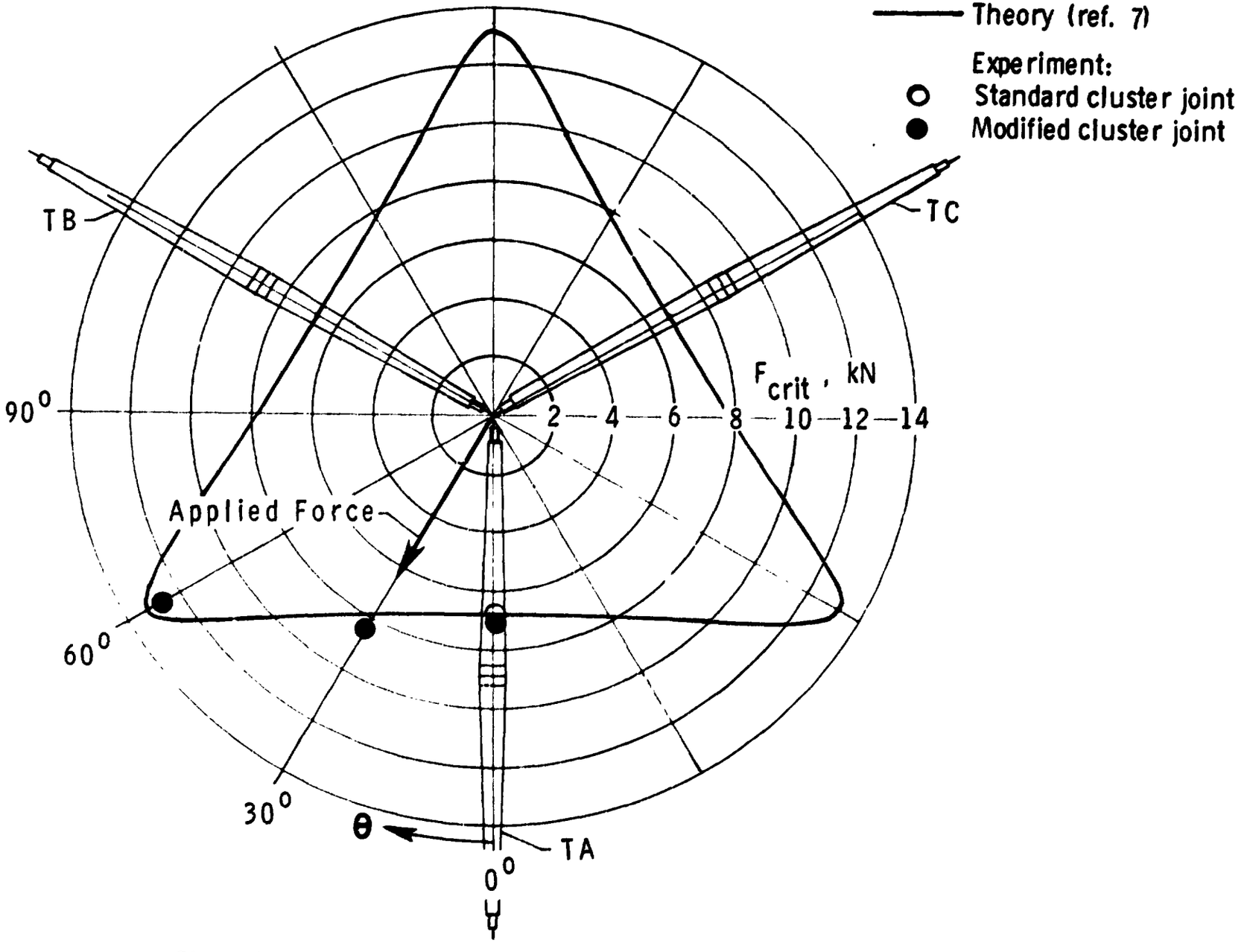

Figure 22.- Comparison of tripod buckling loads with theory.

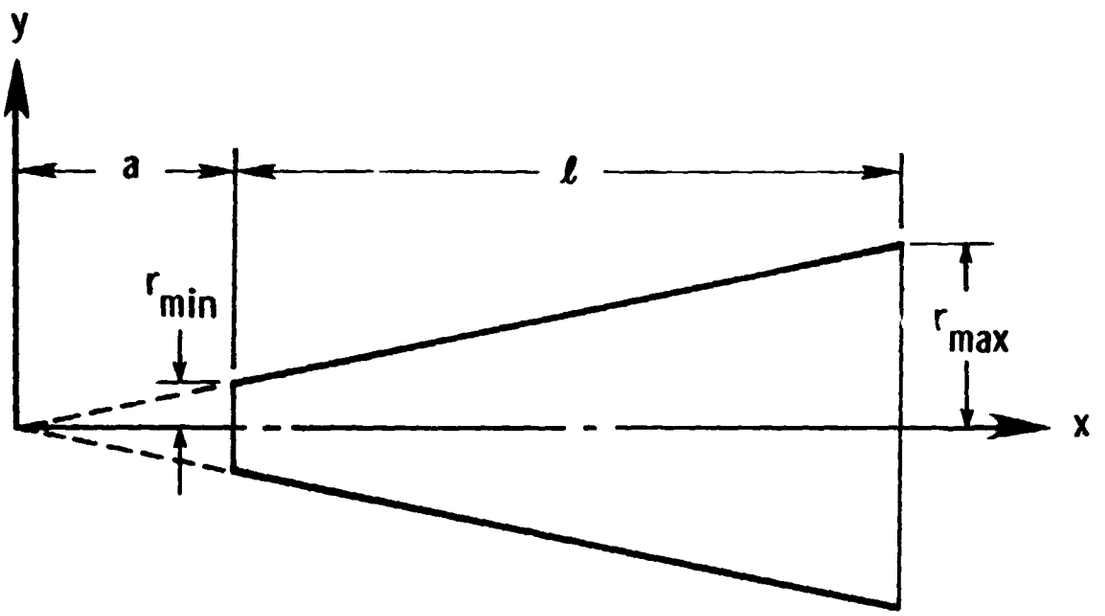

Figure 23.- Geometry and co-ordinate system of tapered tube.